

SCP-2/SCP-x gene ablation alters lipid raft domains in primary cultured mouse hepatocytes[§]

Barbara P. Atshaves,* Avery L. McIntosh,* H. Ross Payne,† Adalberto M. Gallegos,† Kerstin Landrock,* Nobuyo Maeda,§ Ann B. Kier,† and Friedhelm Schroeder^{1,*}

Department of Physiology and Pharmacology,* Texas A&M University, Texas Veterinary Medical Center, College Station, TX 77843-4466; Department of Pathobiology,† Texas A&M University, TVMC, College Station, TX 77843-4467; and Department of Pathology,§ University of North Carolina at Chapel Hill, Chapel Hill, NC 27599-7525

Abstract Although reverse cholesterol transport from peripheral cell types is mediated through plasma membrane microdomains termed lipid rafts, almost nothing is known regarding the existence, protein/lipid composition, or structure of these putative domains in liver hepatocytes, cells responsible for the net removal of cholesterol from the body. Lipid rafts purified from hepatocyte plasma membranes by a nondetergent affinity chromatography method were: *i*) present at $33 \pm 3\%$ of total plasma membrane protein; *ii*) enriched in key proteins of the reverse cholesterol pathway [scavenger receptor class B type I (SR-B1), ABCA1, P-glycoprotein (P-gp), sterol carrier protein-2 (SCP-2)]; *iii*) devoid of caveolin-1; *iv*) enriched in cholesterol, sphingomyelin, GM1, and phospholipids low in polyunsaturated fatty acid and double bond index; and *v*) exhibited an intermediate liquid-ordered lipid phase with significant transbilayer fluidity gradient. Ablation of the gene encoding SCP-2 significantly altered lipid rafts to: *i*) increase the proportion of lipid rafts present, thereby increasing raft total content of ABCA1, P-gp, and SR-B1; *ii*) increase total phospholipids while decreasing GM1 in lipid rafts; *iii*) decrease the fluidity of lipid rafts, consistent with the increased intermediate liquid-ordered phase; and *iv*) abolish the lipid raft transbilayer fluidity gradient. Thus, despite the absence of caveolin-1 in liver hepatocytes, lipid rafts represented nearly one-third of the mouse hepatocyte plasma membrane proteins and displayed unique protein, lipid, and biophysical properties that were differentially regulated by SCP-2 expression.—Atshaves, B. P., A. L. McIntosh, H. R. Payne, A. M. Gallegos, K. Landrock, N. Maeda, A. B. Kier, and F. Schroeder. SCP-2/SCP-x gene ablation alters lipid raft domains in primary cultured mouse hepatocytes. *J. Lipid Res.* 2007. 48: 2193–2211.

Supplementary key words sterol carrier protein • SR-B1 • reverse cholesterol transport • ABCA1

Although all cells synthesize cholesterol, only liver and steroidogenic tissues effect net cholesterol removal. Re-

verse cholesterol transport (RCT) from peripheral tissues to liver for oxidation and excretion is the major physiological pathway for the net cholesterol elimination from the body. Although increasing evidence indicates that plasma membrane microdomains, termed lipid rafts/caveolae, compartmentalize cell surface proteins that mediate HDL-cholesterol uptake/efflux in peripheral cells, the existence and/or significance of such domains in hepatocyte plasma membranes is not completely clear, especially in view of the nearly negligible levels of caveolin-1 in liver. However, an overall scheme is beginning to evolve based largely on findings with peripheral cells (reviewed in Ref. 1).

First, peripheral cells (fibroblasts, muscle, and endothelial cells) are rich in both lipid rafts and caveolae (a subset of lipid rafts rich in several components of the RCT pathway) but are relatively poor in intracellular cholesterol binding proteins such as sterol carrier protein-2 (SCP-2) that facilitate cholesterol retention rather than efflux (reviewed in Refs. 1, 2). Cholesterol effluxes from peripheral cells to HDL by a process facilitated by: *i*) the HDL receptor scavenger receptor class B type I (SR-B1) (3); *ii*) ABCA1, a protein that mediates cholesterol and phosphatidylcholine desorption from the plasma membrane to apolipoprotein A-I (apoA-I) in the plasma, thereby leading to the formation of HDL (4); and *iii*) P-glycoprotein (P-gp), a protein thought to translocate cho-

Abbreviations: apoA-I, apolipoprotein A-I; *cis*-parinaric acid, 9Z,11E,13E,15Z-octatetradecanoic acid; ConA, concanavalin A; DBI, double bond index; DHE, dehydroergosterol; DPH, 1,6-diphenyl-1,3,5-hexatriene; DPH-Pro, 3(1,6-diphenyl-1,3,5-hexatrienyl)-propionic acid; DPH-TMA, 1,6-diphenyl-1,3,5-hexatrienyl-trimethylammonium; eNOS, endothelial nitric oxide synthase; L-FABP, liver fatty acid binding protein; NBD-stearic acid, 12-(*N*-methyl)-*N*[(7-nitrobenz-2-oxa-1,3-diazol-4-yl)amino]-octadecanoic acid; PA, phosphatidic acid; PC, choline glycerophospholipid; PE, ethanolamine glycerophospholipid; P-gp, P-glycoprotein; PI, phosphatidylinositol; PS, phosphatidylserine; RCT, reverse cholesterol transport; SCP-2, sterol carrier protein-2; SM, sphingomyelin; SR-B1, scavenger receptor class B type I.

¹To whom correspondence should be addressed.

e-mail: fschroeder@cvm.tamu.edu

§The online version of this article (available at <http://www.jlr.org>) contains supplementary data in the form of one figure and five tables.

Manuscript received 28 February 2007 and in revised form 29 May 2007 and in re-revised form 13 June 2007.

Published, *JLR Papers in Press*, July 3, 2007.
DOI 10.1194/jlr.M700102-JLR200

lesterol from the cytofacial to the exofacial leaflet of the plasma membrane, facilitating cholesterol efflux to HDL (5).

Second, although HDL transports cholesterol and cholesteryl ester through the vasculature to liver hepatocytes for uptake, it is unclear at present whether this process is mediated through putative lipid rafts in the hepatocyte plasma membrane. In addition, although liver expresses SR-B1, ABCA1, and P-gp, it is not known whether: *i*) hepatocyte plasma membranes contain lipid rafts; *ii*) caveolin-1, highly expressed in liver nonparenchymal cells (e.g., endothelial, stellate, and Kupffer cells), is present in the putative hepatocyte lipid rafts; or *iii*) proteins essential for HDL-mediated cholesterol/cholesteryl ester transport (SR-B1, ABCA1, and P-gp) are present in the putative hepatocyte lipid rafts.

Third, hepatocytes are essentially deficient in caveolin-1 (6–8) but rich in cholesterol binding/transport proteins, including SCP-2 [also liver fatty acid binding protein (L-FABP)], which enhance cholesterol uptake, intracellular retention (esterification), and transport for secretion into bile (reviewed in Ref. 1). Because HDL-mediated cholesterol transport is bidirectional, hepatocytes contain a complement of proteins that not only facilitate efficient cholesterol transport into hepatocytes but also prevent retrograde efflux of cholesterol out of the hepatocyte. Recent real-time fluorescence imaging of sterol transport (9) as well as other studies indicate that hepatocyte intracellular cholesterol transport for secretion into bile is protein-mediated rather than vesicular (reviewed in Ref. 1). Because caveolin-1 is very low/absent in hepatocytes, two other cholesterol binding proteins have been proposed as serving in intracellular cholesterol transport: SCP-2 and L-FABP (reviewed in Ref. 1). In vitro and intact cell studies show that SCP-2 enhances sterol transfer from the plasma membrane to the endoplasmic reticulum and to other intracellular membranes, whereas L-FABP more weakly enhances sterol transfer (reviewed in Ref. 10).

The purpose of the present investigation was to demonstrate: *i*) the existence of lipid rafts in hepatocyte plasma membranes; *ii*) the compartmentalization of RCT proteins therein; *iii*) the unique lipid distribution and structural properties of hepatocyte lipid rafts; *iv*) how these properties of hepatocyte lipid rafts differ from those of nonraft domains; and *v*) whether the cholesterol binding/transfer protein SCP-2 differentially regulates intrinsic properties of hepatocyte lipid rafts. These issues were addressed by the successful application of an affinity chromatography method (11–14) used for the first time on mouse hepatocyte primary cell cultures to simultaneously isolate lipid rafts and nonrafts from purified plasma membranes (derived from wild-type and SCP-2/SCP-x gene-ablated mice) without the use of detergents or high-pH carbonate buffers. In addition, the data showed for the first time that, despite the near absence of caveolin-1 in liver, lipid rafts comprise a substantial portion (nearly one-third based on protein) of the hepatocyte plasma membrane, are enriched in key proteins mediating RCT, and exhibit unique lipid composition and structure compared with nonrafts,

and these properties were regulated in part by the expression of SCP-2.

MATERIALS AND METHODS

Materials

Concanavalin A (ConA) Sepharose resin was purchased from Pharmacia (Piscataway, NJ). Neutral lipid and fatty acid standards were purchased from Nu-Chek Prep, Inc. (Elysian, MN). Phospholipid standards were obtained from Avanti (Alabaster, AL). Silica Gel G and Silica Gel 60 TLC plates were from Analtech (Newark, DE) and EM Industries, Inc. (Darmstadt, Germany), respectively. Rabbit polyclonal antisera to recombinant human SCP-2 were prepared as described previously (15). Rabbit polyclonal antisera to caveolin-1, endothelial nitric oxide synthase (eNOS), and flotillin were from BD Transduction Laboratories (Palo Alto, CA). Rabbit anti-SR-B1 and anti-ABCA1 were from Novus Biologicals (Littleton, CO). Rabbit anti-cholera toxin B and anti-Gq α were from Sigma (St. Louis, MO). Rabbit anti-CXCR4 was purchased from Abcam (Cambridge, MA). Rabbit anti-MDR (P-gp) was from Santa Cruz Biotechnology, Inc. (Santa Cruz, CA). Lowicryl HM20 resin and goat anti-rabbit IgG conjugated to 15 nm gold were from Electron Microscopy Sciences (Fort Washington, PA). 1,6-Diphenyl-1,3,5-hexatriene (DPH), 1,6-diphenyl-1,3,5-hexatrienyl-trimethylammonium (DPH-TMA), 3(1,6-diphenyl-1,3,5-hexatrienyl)-propionic acid (DPH-Pro), 9Z,11E,13E,15Z-octatetradecanoic acid (*cis*-parinaric acid), and 12-(*N*-methyl)-*N*-[(7-nitrobenz-2-oxa-1,3-diazol-4-yl)amino]octadecanoic acid (NBD-stearic acid) were from Molecular Probes (Eugene, OR). Dehydroergosterol (DHE) was synthesized in our laboratory as described previously (16). All reagents and solvents used were of the highest grade available and were cell culture tested.

Animals

All animal protocols were approved by the Institutional Animal Care and Use Committee at Texas A&M University. Male and female (6 weeks old, 20–30 g) inbred C57BL/6Ncr mice were obtained from the National Cancer Institute (Frederick Cancer Research and Developmental Center, Frederick, MD). SCP-2/SCP-x gene-ablated mice were generated as described below. All mice were kept under a 12 h light/dark cycle in a temperature-controlled facility (25°C) with access to food (standard rodent chow mix, 5% fat calories) and water ad libitum. Animals in the facility were monitored quarterly for infectious diseases.

Generation of SCP-2/SCP-x gene-ablated mice

SCP-2/SCP-x gene-ablated mice were generated by targeted disruption of the SCP-2 gene through homologous recombination. The targeting construct was designed to replace exon 16 with the neomycin cassette of the pUnivec-HPRT vector (a generous gift from Dr. Ramiro Ramírez-Solis, Department of Molecular and Human Genetics, Baylor College of Medicine, Houston, TX). Briefly, a genomic 129/sv Lambda FIX[®] library (Stratagene, La Jolla, CA) was screened with a 150 bp DNA fragment containing exon 16 of the SCP-2/SCP-x gene. Positive clones were confirmed by extensive restriction mapping and sequence analysis. Two consecutive genomic DNA fragments, a 2.0 kb *Pst*I clone (containing intronic sequences upstream of exon 16) and a 4.5 kb *Pst*I clone (containing intronic sequences immediately upstream of exon 16, exon 16 itself, and intronic sequences downstream of exon 16) formed the backbone of the targeting construct. The 3' homology arm was generated by ligating a blunt-ended 2.6 kb *Xba*I fragment from the 4.5 kb *Pst*I

clone into Litmus 39 vector (New England Biolabs, Ipswich, MA) predigested with *EcoRV*. This plasmid was digested with *SacI/PstI* and ligated with an 875 bp fragment from the 4.5 kb *PstI* clone digested with *SacI/PstI*. The resulting vector was digested with *BamHI/HindIII* to give a 2,824 bp fragment that was ligated into the pGEM-3Zf vector (Promega, Madison, WI) predigested with *BamHI/HindIII*. Digestion with *EcoRI/HindIII* released the 3' homology region (with an incorporated *KpnI* site later used for Southern blot screening). The 3' homology fragment was blunt-ended with T4 DNA polymerase and ligated into the pUnivc-HPRT vector (predigested with *NotI* and blunted with T4 DNA ligase) to yield an intermediate targeting construct named pUni+3' vector. The 5' homology region was prepared by digesting the 4.5 kb *PstI* clone with *AccI/PstI* to isolate a 2,562 bp fragment that was then ligated to an *AccI/PstI* fragment isolated from the 2.0 kb *PstI* clone. Digestion with *BamHI/AccI* released the 5' homology fragment. The targeting construct was completed by blunt-end ligation of the 5' arm into the intermediate construct pUni+3' vector (predigested with *NheI* and then blunted with T4 DNA polymerase).

Once complete, the targeting construct was opened with *Clat* and electroporated into a 129/Ola-derived embryonic stem cell line E14 maintained on feeder layers. After selection with G418 (200 μ g/ml) and gancyclovir (2 μ M), DNA was isolated from surviving clones, digested with *KpnI*, and screened by Southern blot analysis according to standard protocols. Using a 200 bp 5' probe external to the targeting construct, targeted clones were identified by the presence of a 6 kb band indicating that exon 16 was replaced with the neomycin cassette of pUnivc-HPRT vector. Three positive clones were expanded and injected into C57BL/6Ncr blastocysts to create chimeric mice by standard procedures. Three male chimeras were identified by coat color and bred to C57BL/6Ncr females to determine germline transmission of the targeted allele. Tail DNA from mixed coat-colored (agouti) F1 offspring was screened by PCR to verify the genotype of each animal. Initial characterization of the SCP-2/SCP-x gene ablation by Western analysis was performed on F2 SCP-2^{-/-} homozygous mice generated by interbreeding heterozygous F1 animals. The heterozygous F1 animals were backcrossed to a N6 C57BL/6Ncr background before interbreeding to produce the SCP-2/SCP-x null mice used in this work.

Hepatocyte isolation and culture

Primary cultured hepatocytes derived from the livers of 12 week old male SCP-2/SCP-x null and wild-type mice were isolated as described earlier (17). Primary hepatocytes cultured for ≤ 4 days retain viability and function, as indicated by their undiminished ability to synthesize and secrete albumin (17), synthesize and secrete apolipoproteins (apoA-I, apoE1, and apoB), synthesize L-FABP, secrete lipoproteins (VLDL and HDL), take up fatty acid, transport fatty acid intracellularly, and oxidize fatty acid (17, 18). Therefore, all experiments were performed with hepatocytes maintained in culture for < 2 days, well within the range established for retaining function and viability.

Lipid raft and nonraft isolation from primary cultured hepatocytes

Lipid rafts and nonrafts were isolated from mouse hepatocyte primary cell cultures by a nondetergent, affinity chromatography method developed previously and applied to other cell types (11–14). In brief, for each preparation, hepatocytes (7×10^6 cells/dish), cultured in 150 mm \times 25 mm Corning tissue culture dishes (30 dishes; Corning and Costar, Corning, NY), were washed two times with chilled PBS (4°C) and then scraped into PBS containing protease inhibitor. The hepatocytes were then

sedimented at 1,000 g for 5 min (JA-12 conical rotor and Avanti J-25 centrifuge; Beckman Instruments, Fullerton, CA) at 4°C followed by resuspension in 12 ml of buffer A (0.25 M sucrose and 5 mM Tris-HCl, pH 7.8, 4°C) and disruption with 40 p.s.i. of N₂ for 13 min in an N₂ Bomb Cell Disrupter (Parr Instrument Co., Moline, IL). The postnuclear supernatant was collected after centrifugation, placed on top of 30% Percoll in sucrose/Tris (4°C), and centrifuged at 70,000 g for 30 min (SW40Ti rotor and XL90 ultracentrifuge; Beckman Instruments) at 4°C as described previously (12). The plasma membrane-enriched fraction, located at the interphase between the Percoll and sample layers, was identified by screening all of the visible protein bands separated by the Percoll gradient for the presence of plasma membrane protein markers (transferrin receptor, SR-B1, and Na⁺K⁺-ATPase). Once collected, the enriched plasma membrane fraction was sonicated by three brief 15 s pulses over 3 min with a Fisher 550 Sonic Dismembrator (Fisher Scientific, Pittsburgh, PA) to break up large sheets of plasma membrane. As shown previously by electron microscopy, the disrupted plasma membranes appeared as vesicles (average diameter of 99 nm) or as smaller, broken structures (14). The sonicated plasma membrane fraction was then mixed with ConA Sepharose resin (100 ml) in buffer X (10 mM HEPES, pH 7.4, 140 mM KCl, 1 mM MgCl₂, and 1 mM MnCl₂), incubated under bubbling N₂ for 5 min at 4°C to allow thorough mixing and maximum interface between sample and resin, and then incubated for an additional 15 min without N₂ bubbling.

The solution was poured into a column and left to stand for another 15 min at 4°C. The column was eluted under bubbling N₂ at a rate of 2 ml/min, and 10 ml fractions were collected until the absorbance at 280 nm was close to zero. Based on the enrichment of nonraft marker proteins (CXCR4) and the absence/reduced level of lipid raft markers (flotillin-1, SR-B1, Gq α , and GM1), the eluent was designated as "nonraft." ConA-adherent fractions were then eluted under bubbling N₂ with buffer Y (buffer X plus 0.75 M α -methylmannoside) and were collected at 4°C in 10 ml fractions at 2 ml/min until the absorbance at 280 nm reached a plateau. Based on the enrichment of lipid raft markers (flotillin-1, Gq α , SR-B1, and GM1) and the absence/reduced level of the nonraft marker (CXCR4), the fraction eluting with buffer Y was designated as "lipid raft." Fractions rich in lipid raft markers and nonraft markers were pooled separately and concentrated with Amicon Ultra-15 centrifuge filters (Ultracel 10K; Millipore Corp., Billerica, MA) as indicated by the manufacturer.

The method described above using affinity chromatography to resolve nonrafts and lipid rafts from purified plasma membranes avoided the use of detergents or high-pH carbonate buffers and was the method of choice in the present work for the following reasons. *i*) The affinity chromatography method is the only method that simultaneously isolates lipid rafts and nonrafts from purified plasma membranes (1, 11–14). *ii*) Direct comparison of the properties of lipid rafts isolated by this affinity chromatography method versus the classic Triton X-100 detergent method showed that the affinity chromatography produced lipid rafts that structurally and functionally most closely resembled those of intact cells (13). *iii*) Lipid rafts isolated by the affinity chromatography method exhibited the least amount of nonraft and intracellular contaminants. Mass spectrometry-based proteomics (19) and Western blotting (13, 14) demonstrate that detergent-resistant membranes may contain 30–60% cross-contaminating nonraft and intracellular proteins. Lipid rafts isolated through the use of high-pH bicarbonate buffer may also be highly impure, as shown by MS-based proteomics demonstrating the presence of 75% cross-contaminating nonraft and intracellular proteins (19). *iv*) There is increasing concern that detergent-resistant membranes may not necessarily equate with lipid rafts, quantitatively

reflect the proportion of plasma membrane occurring as lipid rafts, or function as lipid rafts (reviewed in Refs. 1, 13, 20, 21).

Western blot analysis of lipid raft and nonraft fractions

To determine the relative purity of the plasma membrane nonraft and lipid raft fractions eluted from the ConA affinity column, aliquots of each fraction were separated by SDS-PAGE and analyzed by Western blotting (22) to detect relative expression levels of caveolin-1, flotillin, SR-B1, SCP-2, transferrin receptor, CXCR4, eNOS, Gq α , ABCA1, and P-gp. Briefly, 10 μ g of protein (homogenate, plasma membrane, lipid raft, and nonraft) was loaded onto Tricine gels (12%). Gels were run on a Mini-Protean II cell (Bio-Rad Laboratories, Hercules, CA) system at 100 V constant voltage for \sim 1.5–2 h (30 mA per gel initially). Proteins were electrophoretically transferred to nitrocellulose membranes (Bio-Rad) by applying a 100 V constant voltage for 2 h. After transfer, the blots were blocked in 3% gelatin in TBST (10 mM Tris-HCl, pH 8, 100 mM NaCl, and 0.05% Tween-20) for 1 h at room temperature. The blots were then washed twice with TBST and incubated overnight at room temperature with the respective polyclonal rabbit primary antibodies at dilutions of 1:250 (anti-flotillin, anti-ABCA1, anti-P-gp, and anti-SR-B1), 1:500 (anti-SCP-2, anti-caveolin-1, anti-eNOS, and anti-CXCR4), or 1:1,000 (anti-Gq α and anti-transferrin receptor) in 1% gelatin in TBST. The blot was then washed three times with TBST and incubated for 2 h at room temperature with the appropriate secondary antibody (alkaline phosphatase conjugates of goat anti-rabbit IgG) diluted 1:4,500 in 1% gelatin TBST.

Next, the blot was washed three times with TBST and bands of interest were visualized by development with Sigma Fast 5-bromo-4-chloro-3-indolyl phosphate/nitroblue tetrazolium tablets (Sigma) according to the manufacturer's protocol. Images of each blot were acquired using a single-chip charge-coupled device video camera and a computer workstation (IS-500 system; Alpha Innotech, San Leandro, CA). Densitometric analysis of image files was then performed (mean eight bit gray scale density) using NIH Image, available by anonymous FTP from zippy.nimh.nih.gov, to obtain relative levels of the respective proteins detected in each fraction. SCP-2 levels were obtained by comparison with standard curves of known amounts of pure SCP-2 on the same blot. After densitometric analysis of both the standard curve and unknowns on Western blots, image intensities in unknowns were quantitated by comparison with an SCP-2 standard curve within the linear range. For those proteins for which no source of pure protein was available (caveolin-1, flotillin, SR-B1, transferrin receptor, CXCR4, eNOS, Gq α , ABCA1, and P-gp), relative protein levels were quantified as described above and expressed as integrated density values.

Immunoelectron microscopy

Small segments of liver tissue from a female wild-type mouse were fixed by immersion in alcohol-free 4% formaldehyde and 0.1% glutaraldehyde in 0.1 M Na phosphate buffer (pH 7.4) for 20 h at 4°C. The tissue segments were washed in 0.1 M Na phosphate buffer, dehydrated in an ascending ethanol gradient at progressively lower temperatures (23), infiltrated overnight at -50°C with Lowicryl HM20 acrylic resin, and polymerized by UV light. Ultrathin sections (60–80 nm) of liver were mounted on Formvar/carbon-coated nickel grids and immunostained by procedures recommended in the immunogold reagent product literature (Aurion, Wageningen, The Netherlands) with several modifications. Briefly, grids were incubated for 20 min in blocking solution of 1% acetylated BSA (Aurion) in 20 mM Tris-buffered saline and 0.05% Tween-20 (TBS-Tween), pH 7.35, and rinsed in TBS-Tween. Grids were incubated in rabbit anti-caveolin-1 antiserum diluted 1:50 in TBS-Tween with 0.1% BSA

for 18 h at 4°C. After washing six times with TBS-Tween and 0.1% BSA, the grids were incubated for 2 h at 24°C with goat anti-rabbit IgG conjugated to 15 nm gold (Aurion) diluted 1:75 in TBS-Tween and 0.1% BSA. Unbound antibodies were removed from the sections by washing six times with TBS-Tween and 0.1% BSA, then the grids were rinsed with deionized water and post-stained very briefly with aqueous uranyl acetate and Reynold's lead citrate. Immunogold labeling patterns on cells were examined at 80 kV with a Zeiss 10c transmission EM (Carl Zeiss Microimaging, Inc., Thornwood, NY).

Lipid extraction and analysis

Ganglioside GM1 levels were determined by a dot-blot technique as described elsewhere (12). Lipids from homogenate, lipid raft, and nonraft fractions were resolved into individual lipid classes as described (12). In brief, samples were extracted with n-hexane-2-propanol (3:2, v/v), spotted onto Silica Gel G TLC plates, and developed in petroleum ether-diethyl ether-methanol-acetic acid (90:7:2:0.5, v/v/v/v) (24). Neutral lipid content including total cholesterol, FFA, and cholesteryl ester was determined by the method of Marzo et al. (25). Total phospholipids, which included choline glycerophospholipid (PC), sphingomyelin (SM), ethanolamine glycerophospholipid (PE), phosphatidic acid (PA), phosphatidylinositol (PI), and phosphatidylserine (PS), were scraped from the Silica Gel G TLC plates and eluted using chloroform/methanol/HCl (100:50:0.375, v/v/v). Samples were dried under N_2 and resuspended in chloroform. Half of each sample was used for phospholipid fatty acid mass analysis and half was applied to Silica Gel 60 TLC plates to resolve individual phospholipids using chloroform-methanol-water-acetic acid (150:112.5:6:10.5, v/v/v/v). Phospholipid spots were visualized by iodine vapor and identified by comparison with known standards (26). Individual phospholipids were quantitated densitometrically as described (27) and confirmed by phosphorus estimation (28).

Both methods yielded similar quantity and percentage distribution of phospholipid classes. In brief, quantitative analysis was performed by analyzing spot intensity (as for proteins in Western blotting) and compared with linear phospholipid standard curves generated with the same TLC plate to determine phospholipid mass (27). Phospholipid identity was verified by comparison with known phospholipid standards and by lipid phosphorus assay (28). In several fractions, two SM bands were separated on the TLC plate, as reported by other investigators (29). The upper band (SM2) was differentiated from PC (next in order of resolution from the bottom of the TLC plate) by comparison with known phospholipid standards, by lipid phosphorus estimation (28), and was confirmed by GC-MS, noting the differences in the phospholipid fatty acid composition of SM versus PC. The SM fraction was composed of little to no PUFAs and exhibited a prevalence of 20:0, 22:0, 24:0, and 24:1 versus the PC fraction, with substantial levels of PUFAs, including 18:2, 20:4, and 22:6 (29). When comparing SM2 versus SM1, the longer chain fatty acids partitioned more into SM2, including 22:0, 24:0, and 24:1, whereas SM1 was composed of mostly 16:0, 18:0, 18:1, and 20:0 (29). Protein concentration was determined by the method of Bradford (30) from the dried protein extract residue digested overnight in 0.2 M KOH. Lipids were stored under an atmosphere of N_2 to limit oxidation, and all glassware was washed with sulfuric acid-chromate before use.

Phospholipid fatty acid distribution

To obtain the fatty acid composition of each of the major individual phospholipid classes (PC, SM, PS, PI, and PE/PA) in lipid rafts and nonrafts, each phospholipid class was transesterified by acid to convert the phospholipid acyl chains to fatty acid

methyl esters. Individual fatty acid methyl ester species were resolved according to chain length and unsaturation by GC-MS using an RTX-2330 capillary column (0.25 mm i.d. \times 30 m; Restek, West Chester, PA) on a Thermo-Finnigan Trace DSQ single quadrupole mass spectrometer (Thermo Electron Corp., Austin, TX) with electron impact and chemical ionization sources. Injector and detector temperatures were set at 240°C, with a temperature program of 100°C for 1 min, 10°C/min to 140°C, then 2°C/min to 220°C, hold for 1 min, then ramp 20°C/min to 240°C. Individual peaks were identified by comparison with known fatty acid methyl ester standards (Nu-Chek Prep) and referenced against a set concentration of 15:0 added before analysis. Sample identity was confirmed by GC-MS using the Trace DSQ single quadrupole in chemical ionization mode.

Structure of hepatocyte plasma membrane lipid raft and nonraft domains

Fluorescent probes (DHE, *cis*-parinaric acid, NBD-stearic acid, DPH, DPH-TMA, and DPH-Pro), prepared as stock solutions in anhydrous ethanol with 2% (w/v) butylated hydroxytoluene added as an antioxidant, were allowed to incorporate into lipid rafts and nonrafts. Briefly, aliquots of lipid raft or nonraft fractions (35 μ g of protein per 2 ml of 10 nM PIPES buffer, pH 7.4) were incubated at $37 \pm 0.4^\circ\text{C}$ with a small amount of fluorescent probe (protein-fluorophore ratio = 1,000 μ g of protein to 1 μ g of fluorophore) added from a concentrated stock solution in ethanol. The final ethanol concentration was <25 mM, well below that which would perturb membrane structure, lipid distribution, or fluidity (reviewed in Refs. 12, 13, 31), induce artifacts (sterol self-aggregation/crystallization) in membrane fractions (32), or disrupt protein-lipid interactions (33). Maximal probe incorporation was ensured by incubation for 30 min at 37°C . Steady-state fluorescence polarization was acquired with a PC1 spectrofluorometer in the T-format using photon-counting electronics (ISS Instruments, Inc., Champaign, IL) as described previously (13, 31). Polarization data were corrected for residual light scatter by converting polarization to anisotropy ($r = 2P/3P$) and subtracting residual fluorescence anisotropy from all measurements. To avoid inner filter effects, the absorbance of each sample (fluorescent probe + sample) at the wavelength of excitation for each probe was maintained at <0.15 .

The following fluorescent lipidic probe molecules were chosen based on their ability to preferentially report on select aspects of membrane structure: *i*) DHE polarization, to probe the relative fluidity of sterol in lipid rafts and nonrafts (13, 31, 32); *ii*) DPH polarization, to probe for the presence of intermediate liquid-ordered phase lipids (reviewed in Ref. 34); *iii*) *cis*-parinaric acid and NBD-stearic acid polarization, to probe the acyl chain fluidity of naturally occurring and synthetic fatty acids, respectively (reviewed in Ref. 12); and *iv*) DPH-TMA and DPH-Pro polarization, to selectively probe the fluidity of the hydrophobic acyl chain region of lipids in the outer (exofacial) and inner (cytofacial) leaflets of plasma membranes, respectively, (i.e., transbilayer fluidity gradient). The leaflet selectivity of each of the probes (i.e., transbilayer distribution) within isolated plasma membrane fragments was verified by leaflet-selective quenching studies performed as reviewed in Refs. 35, 36 and detailed in the following individually cited papers showing that the inner and outer leaflets of isolated plasma membrane vesicles/fragments differ in fluidity: *i*) leaflet-selective quenching of DPH (nonselectively partitions into both leaflets) (37–39); *ii*) studies with right side-out and inside-out plasma membranes (38); *iii*) studies with the leaflet-selective DPH derivatives DPH-TMA and DPH-Pro (39), which are anchored closer to the membrane surface than DPH (40); *iv*) spin-label probes and purified

right side-out and inside-out oriented plasma membranes (41); and *v*) model membrane studies of fluidity of outer versus inner leaflet phospholipid mixtures (42). Based on these previous findings, fluorescence polarization of the leaflet-selective DPH derivatives DPH-TMA and DPH-Pro were used to measure the transbilayer fluidity gradient in hepatocyte plasma membrane lipid rafts and nonrafts exactly as described earlier (13, 39). These two plasma membrane vesicle fractions resolved by ConA affinity chromatography are both oriented right side out (11). Although the mechanisms whereby the DPH-TMA and DPH-Pro translocate and distribute selectively across the membrane are not known, it is established that zwitterionic phospholipids (PC and SM) and anionic phospholipids (PS) are enriched in the exofacial and cytofacial leaflets, respectively, as a result of the action of phospholipid flippases and/or scramblases present in the plasma membrane (43, 44). Thus, based on the similarities of charged polar head groups, it may be postulated that DPH-TMA (a zwitterionic polar head group) and DPH-Pro (an anionic polar head group) are translocated by plasma membrane flippases and/or scramblases to distribute similarly to their zwitterionic and anionic phospholipid counterparts. Finally, in support of the finding that leaflet-selective DPH-TMA and DPH-Pro show a more rigid cytofacial leaflet and a more fluid exofacial leaflet (39), studies with a nonflipping ESR probe inserted into right side-out and inside-out oriented plasma membranes confirm the more rigid cytofacial leaflet and more fluid exofacial leaflet (41).

Statistical analysis

All data values are expressed as means \pm SEM ($n = 3-7$). To obtain statistical differences between values, ANOVA combined with the Newman-Keuls multiple comparisons test (GraphPad Prism, San Diego, CA) was performed. Differences at the $P < 0.05$ level were considered statistically significant.

RESULTS

Generation of SCP-2/SCP-x gene-ablated mice

To generate SCP-2/SCP-x null mice, a targeting construct was designed that replaced exon 16 of the SCP-2/SCP-x gene with a neomycin cassette (Fig. 1A). This strategy was based on the fact that the SCP-2/SCP-x gene contains two separate promoters separately encoding the 58 kDa SCP-x protein (composed of exons 1–16) and the 15.2 kDa pro-SCP-2 protein (composed of exons 12–16). Both SCP-x and pro-SCP-2 share the same C terminus (including exon 16), and both are posttranslationally processed to the 13.2 kDa SCP-2, so that ablation of exon 16 removes key sequences, resulting in full deletion of SCP-2 and SCP-x. The gene-targeted mice were screened by Southern blot analysis (Fig. 1B), PCR (Fig. 1C), and Western blot analysis (Fig. 1D). As predicted from the construct design, SCP-2 proteins (the 58 kDa SCP-x, 15.2 kDa pro-SCP-2, and 13.2 kDa SCP-2 derived from proteolytic cleavage of the 15.2 kDa SCP-2 and/or potentially from the 58 kDa SCP-x protein) were undetectable in livers from SCP-2/SCP-x null mice, thus confirming gene ablation.

Affinity chromatography of purified plasma membranes isolated from primary hepatocytes

The first step to isolate lipid rafts and nonrafts from hepatocyte plasma membranes was to purify the plasma

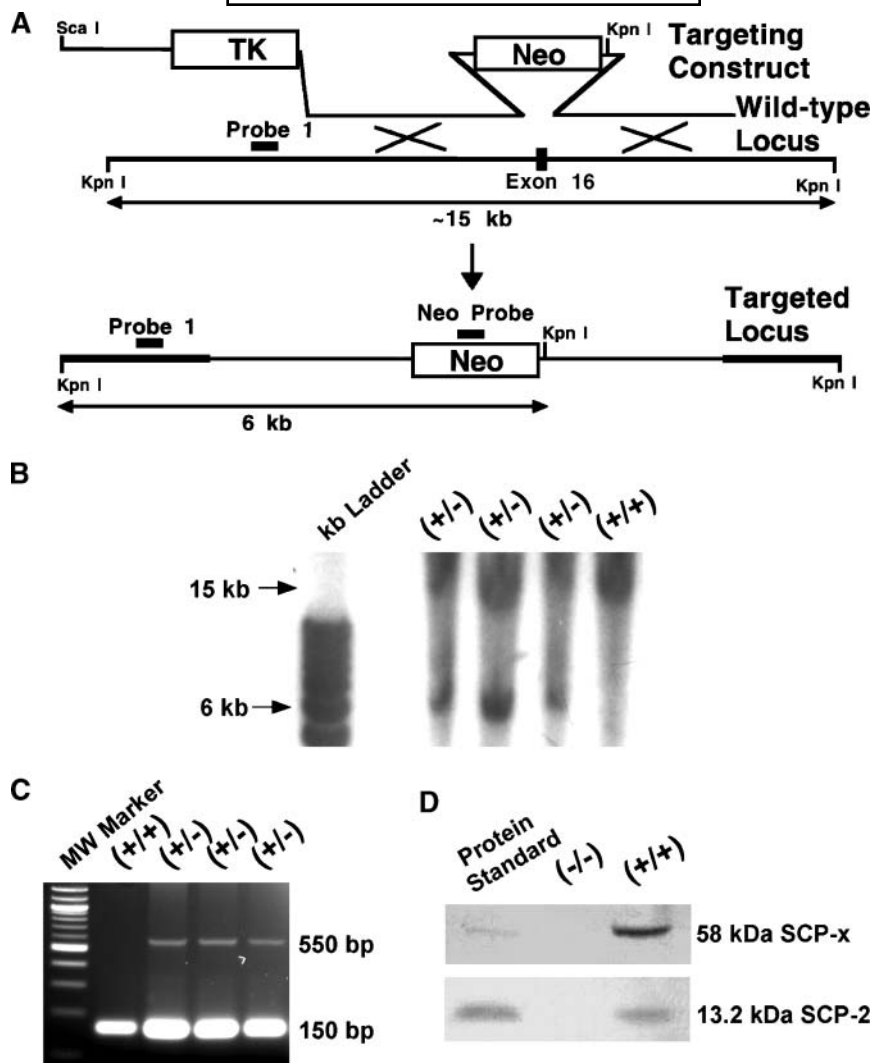


Fig. 1. Generation of the sterol carrier protein-2 (SCP-2)/SCP-x null mouse. A: Targeted mutation of the SCP-2 gene is indicated in the upper diagram. Exon 16 is replaced by a neomycin resistance cassette through homologous recombination. The lower diagram shows the mutated SCP-2 gene with the *KpnI* sites, external probe 1, and Neo probe indicated. B: Southern blot of *KpnI*-digested DNA probed with external probe 1 shows the wild-type (15 kb) and targeted (6 kb) DNA. C: PCR screening of tail DNA from SCP-2/SCP-x wild-type (+/+) and SCP-2/SCP-x heterozygous (+/-) mice. D: Western blot analysis of liver cell homogenates (10 μ g) from SCP-2/SCP-x (-/-) null (lane 2) and wild-type (lane 3) mice probed with an affinity-purified rabbit polyclonal antibody directed against SCP-2, which recognizes SCP-2 and SCP-x gene products. TK indicates thymidine kinase.

membrane, as described in Materials and Methods. Western blot analysis was performed to determine the presence of select protein markers (flotillin, SR-B1, SCP-2, transferrin receptor, and CXCR4) in the hepatocyte homogenate (Fig. 2, lane 1) and in purified plasma membranes (Fig. 2, lane 2) isolated from wild-type mice. Enrichment of flotillin (Fig. 2A) and SR-B1 (Fig. 2B) was observed in the plasma membrane fraction compared with the hepatocyte homogenate. SCP-2 (Fig. 2C), transferrin receptor (Fig. 2D), and CXCR4 (Fig. 2E) were also detected in homogenates and plasma membranes but did not appear to be enriched in the latter. Resolution of the purified plasma membrane fraction by ConA Sepharose affinity chromatography, as described in Materials and Methods,

yielded two fractions, a nonadherent fraction and an adherent fraction (eluted with buffer containing the displacing sugar α -methylmannoside). Enrichment of marker proteins and lipids in the ConA nonadherent and adherent fractions isolated from peripheral cell types (fibroblasts and MDCK cells) previously established these fractions to be enriched in nonrafts and lipid rafts, respectively (1, 12, 13).

In the present work, when the hepatocyte plasma membrane fraction was passed over a ConA Sepharose affinity column, two fractions were obtained: a nonadherent fraction ($67 \pm 5\%$ of total protein) and an adherent fraction ($33 \pm 3\%$ of total protein) (Fig. 3A). Thus, although the nonraft fraction had nearly 2-fold more protein than the

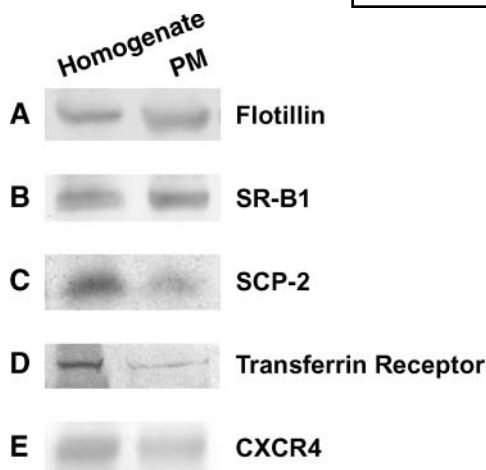


Fig. 2. Western blot analysis of homogenate and plasma membrane proteins in hepatocytes derived from male wild-type SCP-2/SCP-x mice. Levels of flotillin (A) scavenger receptor class B type I (SR-B1) (B), SCP-2 (C), transferrin receptor (D), and CXCR4 (E) were determined by Western blot analysis (see Materials and Methods) in homogenate (lane 1) and plasma membranes (PM; lane 2).

lipid raft fraction in wild-type mice, the lipid raft fraction represented a significant component of the plasma membrane. To determine whether SCP-2/SCP-x gene ablation altered the relative proportion of plasma membrane representing lipid rafts, protein distribution was determined in lipid rafts and/or nonrafts isolated from purified plasma membranes obtained from livers of SCP-2/SCP-x gene-ablated mice (Fig. 3A). The nonadherent, nonraft fraction represented $51 \pm 2\%$ of the plasma membrane protein (significantly less than observed with the wild-type fraction), whereas the ConA adherent lipid raft accounted for $49 \pm 2\%$ of the plasma membrane protein (significantly more than the wild-type fraction). In summary, biochemical fractionation indicated the presence of lipid rafts in the plasma membrane of primary hepatocytes, where they represented a significant proportion. Furthermore, SCP-2/SCP-x gene ablation significantly increased the size of the lipid raft fraction by 48% ($P \leq 0.04$, $n = 6$) at the expense of the nonraft fraction.

Distribution of protein markers in ConA nonadherent and adherent fractions

To confirm that the ConA nonadherent and adherent fractions from hepatocyte plasma membranes indeed represented nonraft- and lipid raft-enriched fractions, Western blotting for marker proteins was performed as described in Materials and Methods to determine the presence of nonraft markers [transferrin receptor (45) and CXCR4 (46)] and lipid raft markers [flotillin (12) and Gq α (47)]. Although the transferrin receptor (also known as CD71) is an excellent protein marker for nonrafts in endothelial cells as well as many different cell lines and primary cells (45, 48, 49), in this work transferrin was not detectable in the nonadherent fraction isolated from primary mouse hepatocytes (data not shown). However, when the nonadherent fraction was tested for another nonraft protein

marker, CXCR4, levels were 10.8-fold greater in the ConA nonadherent fraction compared with the adherent fraction (Fig. 3D). To distinguish whether the nonadherent fraction was deficient in lipid raft protein markers, Western blotting of known lipid raft protein markers (flotillin and Gq α) was also performed. The nonadherent fraction was essentially devoid of flotillin (Fig. 3B, hatched bar) and Gq α (Fig. 3C, hatched bar) compared with either the cell homogenate (Fig. 3, open bars) or the ConA adherent fraction (Fig. 3, closed bars). In contrast, Western blot analysis of the ConA adherent fraction showed >9-fold enrichment in flotillin (Fig. 3B) and 14-fold enrichment in Gq α (Fig. 3C) compared with the nonadherent fraction. In SCP-2/SCP-x gene-ablated mice, with the exception of SCP-2 being absent, the pattern of protein markers for lipid rafts was similar to that in wild-type mice (i.e., enrichment of flotillin and Gq α in lipid rafts and enrichment of CXCR4 in nonrafts). In summary, the Western blotting of protein markers confirmed that the ConA nonadherent and adherent fractions were enriched in nonrafts and lipid rafts, respectively, and expression of SCP-2/SCP-x significantly altered the relative proportion of lipid rafts versus nonrafts in the plasma membrane of primary hepatocytes.

Distribution of lipid markers in the ConA nonadherent and adherent fractions

To further confirm that the ConA nonadherent and adherent fractions from hepatocyte plasma membranes represented nonraft- and lipid raft-enriched fractions, lipid analyses for marker lipids were performed as described in Materials and Methods. Lipid rafts from peripheral cells are known to be enriched in total lipid, cholesterol, phospholipid, and sphingolipids (GM1 and SM) (reviewed in Ref. 13). In this work, the adherent fraction was lipid-rich, as shown by the >3-fold higher total lipid/protein compared with the ConA nonadherent fraction (Fig. 4A). Examination of individual lipid classes from lipid rafts of wild-type mice revealed that the adherent fraction had several-fold more ganglioside GM1 (Fig. 4B), SM (Fig. 4C), total cholesterol (Fig. 4D), and total phospholipids (Fig. 4E) compared with the ConA nonadherent fraction or the cell homogenate. The molar ratio of cholesterol-phospholipid (C/P) was >2-fold higher in the adherent fraction compared with the nonadherent fraction (Fig. 4F).

To determine whether the difference in total phospholipids in the nonraft and lipid raft fractions was attributable to preferential distribution of select phospholipid classes, the mass (nmol/mg protein) and distribution (%) of the individual phospholipid classes, including PC, PS, PI, and PE/PA, were analyzed as described in Materials and Methods. In the cell homogenate of wild-type hepatocytes (Fig. 5A, open bars), the relative distribution of individual phospholipid classes was in the order PC >> PE > PS and PI. When plasma membranes were fractionated into lipid rafts and nonrafts, the masses (nmol/mg protein) of all of the phospholipid classes were substantially lower, but not equally so, in the lipid raft compared with the nonraft fractions (Fig. 5B): the content of PC, PS, PI, and PE in lipid rafts of wild-type hepatocytes was 1.7-, 5.4-,

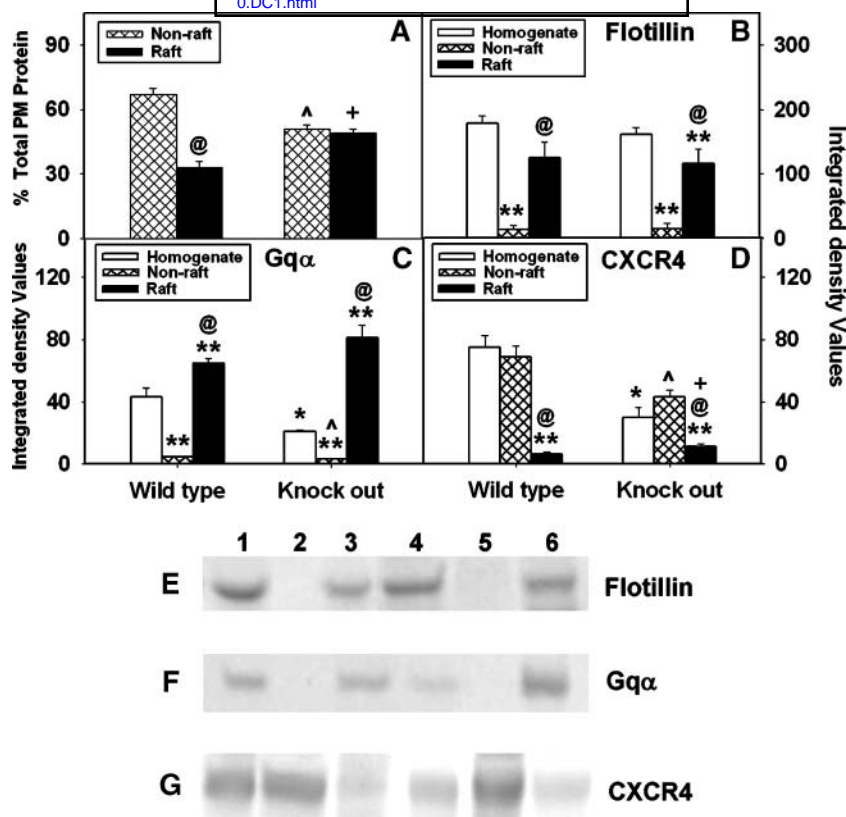


Fig. 3. Distribution of plasma membrane (PM) protein markers in hepatocyte plasma membrane nonraft and lipid raft fractions. A: Total protein distribution in lipid rafts (closed bar) and nonrafts (hatched bar) isolated from wild-type and SCP-2/SCP-x null mice. B–D: Quantitative analysis of protein expression was performed on flotillin (B), Gqα (C), and CXCR4 (D) in homogenate (open bars), nonraft (hatched bars), and lipid raft (closed bars) fractions derived from SCP-2/SCP-x null and wild-type hepatocytes. E–G: Representative Western blots performed on *i*) SCP-2/SCP-x wild-type hepatocyte homogenate (lane 1), nonraft (lane 2), and lipid raft (lane 3) fractions and *ii*) SCP-2/SCP-x null hepatocyte homogenate (lane 4), nonraft (lane 5), and lipid raft (lane 6) fractions to determine expression levels of flotillin (E), Gqα (F), and CXCR4 (G). Values in A–D represent means \pm SEM ($n = 3–6$). * $P < 0.02$ for wild-type (WT) homogenates versus SCP-2/SCP-x null (KO) homogenates; ** $P < 0.05$ for homogenate versus nonraft or lipid raft within each group (WT or KO); @ $P < 0.01$ for nonraft versus lipid raft within each group (WT or KO); + $P < 0.05$ for WT lipid raft versus KO lipid raft; ^ $P < 0.04$ for WT nonraft versus KO nonraft.

3.7-, and 1.9-fold higher than in the nonraft fraction ($P < 0.05$, $n = 3–6$). When expressed as the relative prevalence (%) of polar lipids, individual phospholipid classes were in the order PC ($39 \pm 2\%$) > SM ($21 \pm 2\%$) and PE ($21 \pm 2\%$) > PI ($10 \pm 1\%$) and PS ($10 \pm 1\%$) in lipid rafts isolated from wild-type hepatocytes (Fig. 5C). In nonrafts from wild-type hepatocytes, the relative percentage of PC was significantly higher than in lipid rafts, whereas the nonraft percentage of PI and PS decreased by >50% (Fig. 5C). Thus, in wild-type hepatocytes, the ratio of anionic to neutral zwitterionic phospholipids [i.e., (PS + PI)/(PC + PE + SM)] was >2-fold higher in lipid rafts than nonrafts (Fig. 5D).

To determine whether SCP-2/SCP-x gene ablation altered the lipid composition of hepatocytes, lipids were extracted, resolved by TLC, and quantitated as described in Materials and Methods. Although SCP-2/SCP-x gene ablation did not alter the total mass of lipid (Fig. 4A) or total phospholipid (Fig. 4E) in cell homogenate, the masses of GM1 (Fig. 4B), PS (Fig. 5A), and PI (Fig. 5A) in

cell homogenate were increased by 1.4-, 3.1-, and 2.4-fold, respectively. To determine whether the latter enrichments were selectively reflected in lipid rafts versus nonrafts, the individual lipid classes of these fractions from SCP-2/SCP-x null mice were examined. Although SCP-2/SCP-x gene ablation did not alter the mass of total cholesterol in lipid rafts or nonrafts (Fig. 4D), the total mass of phospholipids was significantly increased by 1.2-fold in lipid rafts and decreased by 50% in nonrafts (Fig. 4E). Consequently, there was no significant difference in the C/P ratio between these fractions isolated from plasma membranes of hepatocytes from SCP-2/SCP-x mice (Fig. 4F). SCP-2/SCP-x gene ablation also significantly decreased the level of the sphingolipid GM1 by 27% (Fig. 4B) and PE by 20% (Fig. 5B) in lipid rafts but not nonrafts. Concomitantly, SM (Fig. 4C), PC (Fig. 5B), and PI (Fig. 5B) increased by 2.4-, 1.4-, and 1.7-fold, respectively, in lipid rafts. With regard to the other individual polar lipid classes, lack of SCP-2/SCP-x did not alter the lipid raft mass (nmol/mg protein) of PS (Fig. 5B).

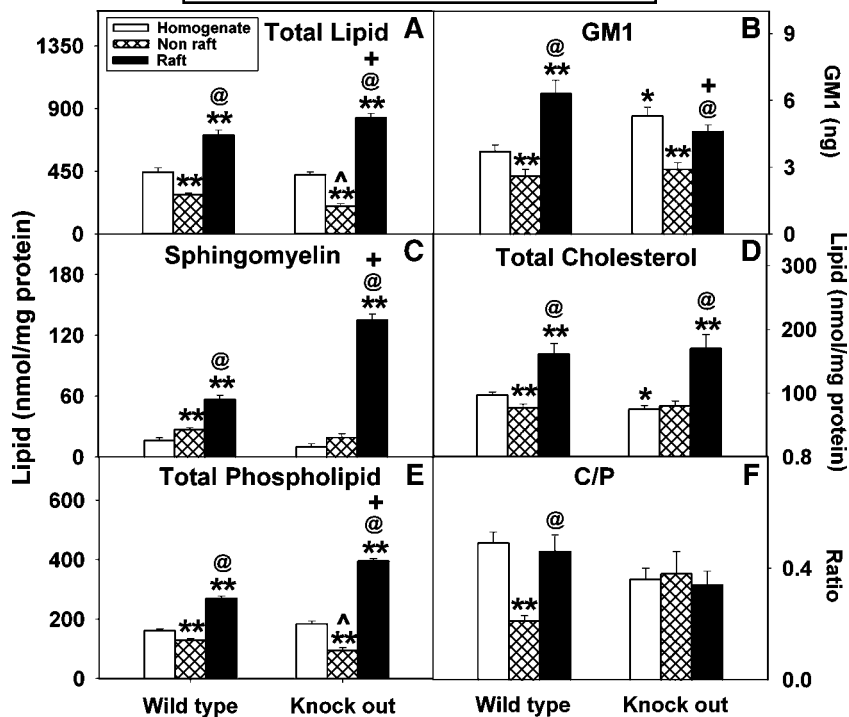


Fig. 4. Distribution of lipid markers in hepatocyte nonraft and lipid raft fractions. Total lipids (A), ganglioside GM1 (B), sphingomyelin (C), total cholesterol (D), total phospholipids (E), and the cholesterol-phospholipid (C/P) ratio (F) were determined in homogenates (open bars), nonrafts (hatched bars), and lipid rafts (closed bars) isolated from SCP-2/SCP-x null and wild-type hepatocytes. Values represent means \pm SEM (n = 3–9). * $P < 0.03$ for wild-type (WT) homogenates versus SCP-2/SCP-x null (KO) homogenates; ** $P < 0.04$ for homogenate versus nonraft or lipid raft within each group (WT or KO); @ $P < 0.03$ for nonraft versus lipid raft within each group (WT or KO); + $P < 0.04$ for WT lipid raft versus KO lipid raft; ^ $P < 0.02$ for WT nonraft versus KO nonraft.

When phospholipid composition was expressed as a percentage, SCP-2/SCP-x gene ablation increased the percentage of SM in lipid rafts while decreasing the percentage of PE versus that in lipid rafts from wild-type hepatocytes (Fig. 5C). In nonraft fractions, lack of SCP-2/SCP-x expression did not significantly affect either the mass (Fig. 5B) or the percentage composition (Fig. 5C) of any of the phospholipid classes examined, with the exception of PI, whose percentage (Fig. 5C) but not mass (Fig. 5B) was increased somewhat. Finally, the overall ratio of anionic to neutral zwitterionic phospholipids was not changed in SCP-2/SCP-x null lipid rafts but increased by 2.4-fold in nonrafts (Fig. 5D) compared with the corresponding fractions from wild-type hepatocytes. In summary, the lipid marker distribution confirmed that the ConA nonadherent and adherent fractions were enriched in nonrafts and lipid rafts, respectively. In wild-type hepatocytes, lipid rafts were enriched in total lipids, total cholesterol, total phospholipids, and cholesterol-to-phospholipid ratio, as well as by mass in polar lipid classes (GM1, PC, SM, PE, PS, and PI), compared with nonrafts. SCP-2/SCP-x gene ablation significantly increased the total lipid content, total phospholipid, and select phospholipid classes (SM, PC, and PI) in lipid rafts. Furthermore, SCP-2 gene ablation abolished the difference in the C/P ratio in lipid rafts versus nonrafts by increasing the

content of total phospholipid in lipid rafts and decreasing the content of total phospholipid in nonrafts, without altering cholesterol mass.

Select distribution of proteins involved in HDL-mediated cholesterol uptake/efflux in lipid rafts

To determine whether key proteins involved in RCT (ABCA1, P-gp, SR-B1, SCP-2, and caveolin-1) were compartmentalized in lipid rafts, Western blotting for the respective proteins was performed. Compared with the nonraft fraction of plasma membranes from hepatocytes, the lipid raft fraction was highly enriched by >100-fold in SCP-2 (Fig. 6A, E), 6.6-fold in ABCA1 (Fig. 6B, F), 7.4-fold in P-gp (Fig. 6C, G), and 11-fold in SR-B1 (Fig. 6D, H). The presence of caveolin-1 was not detected in lipid rafts or nonrafts (Fig. 7A, lanes 2 and 3, respectively). Indeed, although Western blotting detected caveolin-1 in liver homogenates (Fig. 7A, lane 1), the concomitant presence of high levels of eNOS therein (Fig. 7B, lane 2) suggested that caveolin-1 may reside in nonhepatic cells (endothelial, stellate, and Kupffer cells) rather than in hepatocytes. Consistent with this possibility, eNOS (Fig. 7B, lane 3), the transferrin receptor [protein marker present in nonrafts of other cell types (45, 48, 49)], in addition to caveolin-1 (Fig. 7, lanes 2, 3) were absent in lipid raft and nonraft fractions isolated from hepatocyte cells. Because

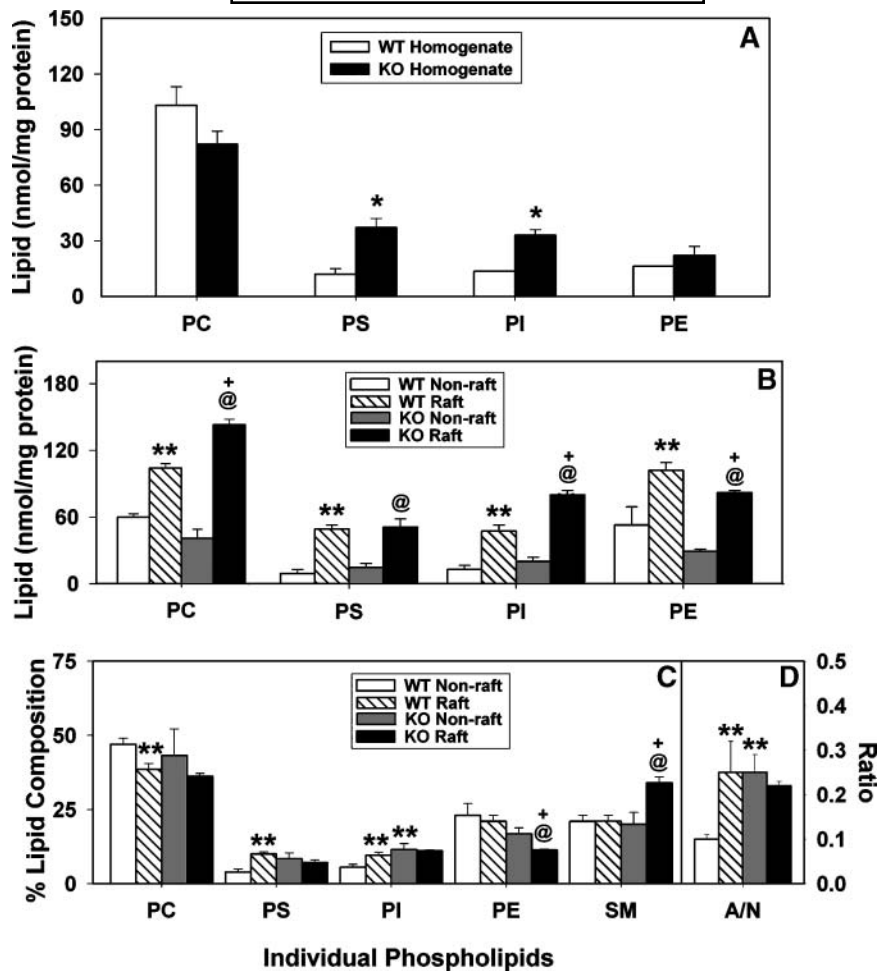


Fig. 5. Distribution of individual phospholipid classes in hepatocyte nonraft and lipid raft fractions. A: Levels of individual phospholipids in homogenates isolated from SCP-2/SCP-x null (closed bars) and SCP-2/SCP-x wild-type (open bars) hepatocytes were determined as described in Materials and Methods. B: Levels of individual phospholipids in SCP-2/SCP-x wild-type nonrafts (open bars) and lipid rafts (hatched bars) and in SCP-2/SCP-x null nonrafts (shaded bars) and lipid rafts (closed bars). C: Percentage composition of individual phospholipids in SCP-2/SCP-x wild-type nonrafts (open bars) and lipid rafts (hatched bars) and in SCP-2/SCP-x null nonrafts (shaded bars) and lipid rafts (closed bars). D: Ratio of anionic to neutral/zwitterionic (A/N) phospholipids in each fraction. PC, choline glycerophospholipid; PE, ethanolamine glycerophospholipid; PI, phosphatidylinositol; PS, phosphatidylserine. Values represent means \pm SEM ($n = 3-6$). * $P < 0.03$ for wild-type (WT) homogenates versus SCP-2/SCP-x (KO) homogenates; ** $P < 0.02$ compared with WT nonraft fraction within each phospholipid; @ $P < 0.001$ compared with KO nonraft fraction within each phospholipid; + $P < 0.05$ compared with WT lipid raft within each phospholipid.

liver contains not only hepatocytes but also a variety of other cells (endothelial, stellate, and Kupffer cells), the latter being enriched in caveolin-1 (50, 51), antigenic sites of caveolin-1 were also localized on thin sections of liver with 15 nm gold particles using immunogold electron microscopy. Multiple sites of caveolin-1 in endothelial cells (Fig. 7C, arrowheads) and other nonparenchymal cell types (data not shown) were observed. In contrast, hepatocytes (Fig. 7D) did not show staining for caveolin-1 above random background levels. These results were consistent with the absence of caveolin-1 from hepatocytes both in mouse hepatocyte primary cell cultures and in vivo.

Distribution of lipids associated with HDL-mediated cholesterol transfer in lipid rafts

In peripheral cells, selective transfer of cholesterol and cholesteryl ester associated with HDL (which binds SR-B1) is mediated through lipid rafts rich in ABCA1, P-gp, and SR-B1 (reviewed in Ref. 13). Because hepatocyte lipid rafts were enriched in ABCA1, P-gp, SR-B1, and SCP-2, the possibility that not only unesterified cholesterol but also small amounts of cholesteryl ester might be detectable in lipid rafts was examined. Compared with the nonrafts, lipid rafts had 4.9-fold more unesterified cholesterol (see supplementary Fig. I) but similar small levels of cholesteryl ester (see supplementary Fig. IB). In addition, lipid rafts

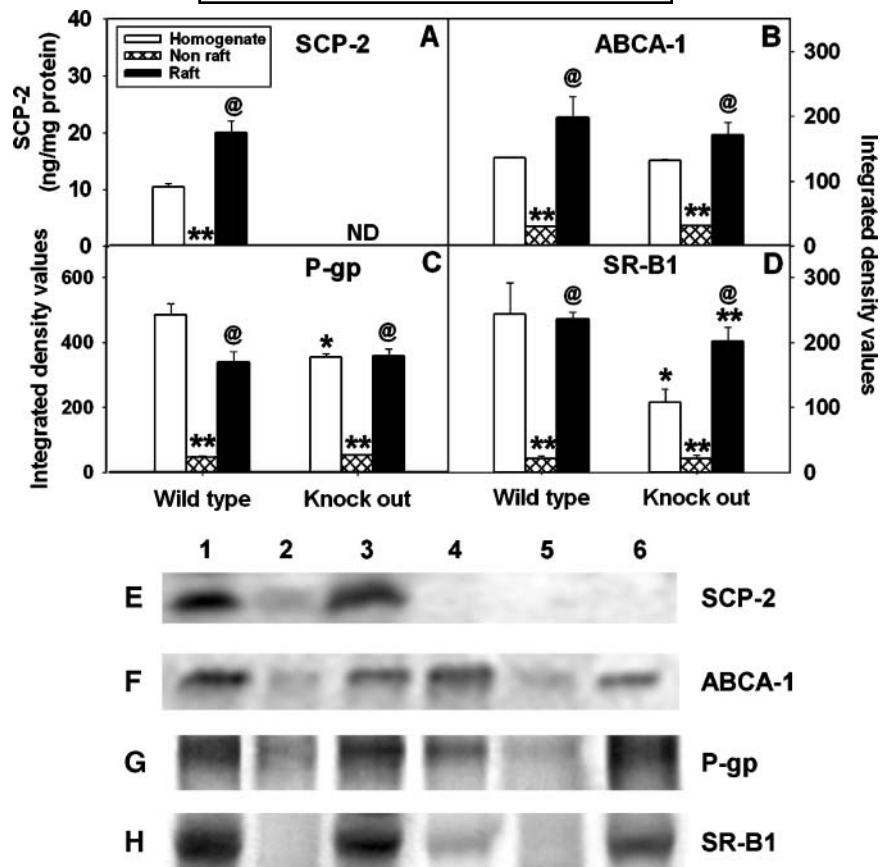


Fig. 6. Expression of proteins involved in HDL-cholesterol trafficking in hepatocyte nonraft and lipid raft fractions. A–D: Quantitative analysis was performed on levels of SCP-2 (A), ABCA1 (B), P-glycoprotein (P-gp) (C), and SR-B1 (D) in homogenate (open bars), nonraft (hatched bars), and lipid raft (closed bars) fractions derived from SCP-2/SCP-x null and wild-type hepatocytes. E–H: Western blot analysis using affinity-purified antibodies developed against SCP-2 (E), ABCA1 (F), P-gp (G), and SR-B1 (H) was performed on the following samples: *i*) SCP-2/SCP-x wild-type hepatocyte homogenate (lane 1), nonraft (lane 2), and lipid raft (lane 3) fractions and *ii*) SCP-2/SCP-x null hepatocyte homogenate (lane 4), nonraft (lane 5), and lipid raft (lane 6) fractions. Values represent means \pm SEM ($n = 3-6$). * $P < 0.05$ for wild-type (WT) homogenates versus SCP-2/SCP-x (KO) homogenates; ** $P < 0.03$ for homogenate versus nonraft or lipid raft within each group (WT or KO); @ $P < 0.01$ for nonraft versus lipid raft within each group (WT or KO).

had 3.5-fold more FFA (see supplementary Fig. 1C) compared with the nonraft fraction, consistent with the enrichment of fatty acid transport proteins in lipid rafts (52).

Distribution of phospholipid polyunsaturated fatty acids that regulate the distribution of proteins to lipid rafts

Select phospholipid classes were next examined. SM of both lipid rafts and nonrafts was relatively enriched in saturated (16:0, 18:0, 20:0, 22:0, and 24:0) and monounsaturated (16:1, 18:1, 20:1, 22:1, and 24:1) fatty acids while being relatively poor in polyunsaturated fatty acids (see supplementary Table I) compared with other phospholipid classes (see supplementary Tables II–IV). For more ready comparison, the individual groups of saturated (Sat), unsaturated (Unsat), monounsaturated, and polyunsaturated fatty acids were summed and the ratios of Sat/Unsat and MUFA/Sat and the double bond index (DBI) were calculated and collated in Table 1. Thus, the DBI (defined as the summation of the mole fraction times

the number of double bonds for each fatty acid) was 2- to 5-fold lower in SM (Table 1) than in other phospholipid classes (Tables 2–4). In SM from wild-type hepatocytes, the Sat/Unsat ratio was significantly higher than in nonrafts (Table 1). SCP-2/SCP-x gene ablation abolished this difference (Table 1). Esterified fatty acids detected in the lipid raft PS class from wild-type hepatocytes also differed significantly from nonrafts (see supplementary Table II). In wild-type hepatocyte lipid rafts, the PUFAs were 2-fold lower, giving rise to a higher Sat/Unsat ratio and a lower DBI compared with the nonraft fraction (Table 2). SCP-2/SCP-x gene ablation increased PUFA and DBI while decreasing the Sat/Unsat ratio in lipid rafts compared with lipid rafts from wild-type hepatocytes (Table 2). Concomitantly, SCP-2/SCP-x gene ablation increased MUFA and the MUFA/Sat ratio in nonrafts compared with nonrafts from wild-type hepatocytes (Table 2). Lastly, SCP-2/SCP-x gene ablation did not significantly alter any of the fatty acid parameters

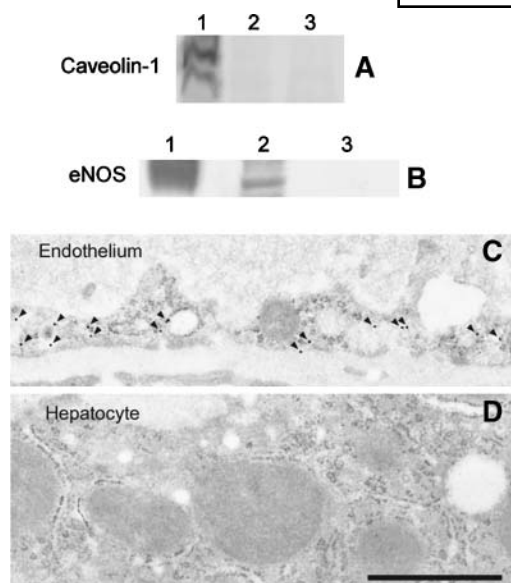


Fig. 7. Distribution of caveolin-1 in hepatocyte plasma membrane lipid rafts (Western blot analysis) and in mouse liver (immunogold electron microscopy). A: Caveolin-1 expression levels in liver homogenate (lane 1), hepatocyte nonraft (lane 2), and hepatocyte lipid raft (lane 3) fractions. B: Expression levels of endothelial nitric oxide synthase (eNOS) in endothelial cells (lane 1; 10 µg), liver homogenate (lane 2; 2 µg), and hepatocyte homogenate (lane 3; 10 µg) determined as described in Materials and Methods. C, D: Antigenic sites of caveolin-1 were immunolabeled with 15 nm gold particles on thin sections of the endothelium (C) and hepatocytes (D). Although numerous sites were immunolabeled for caveolin-1 in endothelial cells, as indicated by arrowheads, only background levels of gold binding to caveolin-1 were observed in hepatocytes. Bar = 1.0 µm.

in raft versus nonraft fractions from SCP-2/SCP-x gene-ablated hepatocytes (Table 2).

With regard to fatty acids esterified to PC, lipid rafts from wild-type hepatocytes also differed significantly from nonrafts (see supplementary Table III). In wild-type hepatocytes, the lipid raft fraction PUFAs were 1.8-fold lower, giving rise to higher Sat/Unsat ratio and lower DBI values versus the nonraft fraction (Table 3). SCP-2/SCP-x gene

TABLE 1. Effect of SCP-2/SCP-x gene ablation on sphingomyelin fatty acid group percentage composition in plasma membrane nonraft and lipid raft fractions

Fatty Acid Group	Nonraft		Raft	
	Wild Type	Knockout	Wild Type	Knockout
Saturated	54 ± 9	56 ± 10	63 ± 6	62 ± 4
Unsaturated	46 ± 4	44 ± 10	38 ± 4	37 ± 3
MUFA	39 ± 4	39 ± 10	32 ± 4	34 ± 4
PUFA	6.8 ± 0.7	5.1 ± 0.6	5.4 ± 0.4	4.9 ± 0.3
Saturated/unsaturated	1.1 ± 0.1	1.3 ± 0.3	1.6 ± 0.2 ^a	1.6 ± 0.1
MUFA/saturated	0.7 ± 0.1	0.7 ± 0.2	0.52 ± 0.07	0.54 ± 0.06
DBI	0.3 ± 0.1	0.2 ± 0.1	0.3 ± 0.1	0.4 ± 0.1

DBI, double bond index; SCP-2, sterol carrier protein-2. Values represent means ± SEM (n = 3–6). See supplementary Table I for the percentage composition of individual sphingomyelin fatty acids.

^aSignificant difference compared with the plasma membrane nonraft fraction isolated from SCP-2/SCP-x wild-type hepatocytes ($P < 0.05$).

TABLE 2. Effect of SCP-2/SCP-x gene ablation on phosphatidylserine fatty acid group percentage composition in plasma membrane nonraft and lipid raft fractions

Fatty Acid Group	Nonraft		Raft	
	Wild Type	Knockout	Wild Type	Knockout
Saturated	53 ± 7	44 ± 5	65 ± 10	51 ± 9
Unsaturated	47 ± 5	56 ± 5	35 ± 6	49 ± 6
MUFA	16 ± 3	30 ± 3 ^a	20 ± 4	23 ± 5
PUFA	32 ± 4	27 ± 3	15 ± 3 ^a	27 ± 4 ^b
Saturated/unsaturated	1.1 ± 0.1	0.78 ± 0.09	1.9 ± 0.3 ^a	1.0 ± 0.2 ^b
MUFA/saturated	0.31 ± 0.04	0.68 ± 0.09 ^a	0.31 ± 0.07	0.45 ± 0.09
DBI	1.2 ± 0.1	0.9 ± 0.1	0.5 ± 0.1 ^a	1.0 ± 0.1 ^b

Values represent means ± SEM (n = 3–6). See supplementary Table II for the percentage composition of individual phosphatidylserine fatty acids.

^aSignificant difference compared with the plasma membrane nonraft fraction isolated from SCP-2/SCP-x wild-type hepatocytes ($P < 0.03$).

^bSignificant difference compared with the plasma membrane lipid raft fraction isolated from SCP-2/SCP-x wild-type hepatocytes ($P < 0.05$).

ablation had no effect on fatty acid parameters in lipid rafts compared with lipid rafts from wild-type hepatocytes (Table 3). Likewise, SCP-2/SCP-x gene ablation had no effect on fatty acid parameters in nonrafts compared with nonrafts from wild-type hepatocytes (Table 3). However, SCP-2/SCP-x gene ablation significantly increased the Sat/Unsat ratio by 1.5-fold in lipid rafts compared with nonrafts from SCP-2/SCP-x gene-ablated hepatocytes (Table 3).

For PI, the esterified fatty acids in lipid rafts from wild-type hepatocytes also differed significantly from nonrafts (see supplementary Table IV). As shown in Table 4, the wild-type lipid raft fraction had lower MUFA, MUFA/Sat ratio, and DBI values, whereas the Sat/Unsat ratio was higher compared with the nonraft fraction. SCP-2/SCP-x gene ablation did not alter fatty acid parameters in lipid rafts compared with lipid rafts from wild-type hepatocytes (Table 4). Likewise, SCP-2/SCP-x gene ablation did not alter these parameters in nonrafts compared with nonrafts from wild-type hepatocytes (Table 4). However, lipid rafts

TABLE 3. Effect of SCP-2/SCP-x gene ablation on phosphatidylcholine fatty acid group percentage composition in plasma membrane nonraft and lipid raft fractions

Fatty Acid Group	Nonraft		Raft	
	Wild Type	Knockout	Wild Type	Knockout
Saturated	50 ± 5	49 ± 7	62 ± 8	61 ± 5
Unsaturated	50 ± 4	51 ± 6	39 ± 4	40 ± 4
MUFA	24 ± 2	31 ± 5	24 ± 4	24 ± 3
PUFA	27 ± 3	19 ± 3	15 ± 2 ^a	16 ± 1
Saturated/unsaturated	1.0 ± 0.1	1.0 ± 0.1	1.6 ± 0.2 ^a	1.5 ± 0.1 ^b
MUFA/saturated	0.48 ± 0.05	0.6 ± 0.1	0.38 ± 0.07	0.39 ± 0.05
DBI	1.0 ± 0.1	0.7 ± 0.1	0.59 ± 0.05 ^a	0.70 ± 0.05

Values represent means ± SEM (n = 3–6). See supplementary Table III for the percentage composition of individual phosphatidylcholine fatty acids.

^aSignificant difference compared with the plasma membrane nonraft fraction isolated from SCP-2/SCP-x wild-type hepatocytes ($P < 0.02$).

^bSignificant difference compared with the plasma membrane nonraft fraction isolated from SCP-2/SCP-x null hepatocytes ($P < 0.02$).

TABLE 4. Effect of SCP-2/SCP-x gene ablation on phosphatidylinositol fatty acid group percentage composition in plasma membrane nonraft and lipid raft fractions

Fatty Acid Group	Nonraft		Raft	
	Wild Type	Knockout	Wild Type	Knockout
Saturated	45 ± 3	44 ± 3	61 ± 12	63 ± 5 ^a
Unsaturated	55 ± 4	56 ± 3	39 ± 6	37 ± 3 ^a
MUFA	27 ± 3	27 ± 2	17 ± 3 ^b	19 ± 2 ^a
PUFA	29 ± 3	29 ± 3	22 ± 4	18 ± 2 ^a
Saturated/unsaturated	0.81 ± 0.06	0.78 ± 0.05	1.6 ± 0.3 ^b	1.7 ± 0.1 ^a
MUFA/saturated	0.59 ± 0.06	0.62 ± 0.04	0.27 ± 0.06 ^b	0.30 ± 0.04 ^a
DBI	1.1 ± 0.1	1.0 ± 0.1	0.80 ± 0.05 ^b	0.7 ± 0.1

Values represent means ± SEM (n = 3–6). See supplementary Table IV for the percentage composition of individual phosphatidylinositol fatty acids.

^aSignificant difference compared with the plasma membrane nonraft fraction isolated from SCP-2/SCP-x null hepatocytes (*P* < 0.01).

^bSignificant difference compared with the plasma membrane nonraft fraction isolated from SCP-2/SCP-x wild-type hepatocytes (*P* < 0.04).

from SCP-2/SCP-x gene-ablated hepatocytes exhibited increased saturated fatty acids and Sat/Unsat ratio concomitant with decreased unsaturated fatty acids, MUFA, PUFA, and MUFA/Sat ratio compared with nonrafts from SCP-2/SCP-x gene-ablated hepatocytes (Table 4).

Esterified fatty acids detected in the lipid raft PE class from wild-type hepatocytes also differed significantly from nonrafts (see supplementary Table V). As summarized in **Table 5**, in wild-type hepatocytes compared with the nonraft fraction, the lipid raft fraction had higher saturated fatty acids and Sat/Unsat ratio but lower unsaturated fatty acids, PUFA, MUFA, and DBI. SCP-2/SCP-x gene ablation had no effect on fatty acid parameters in lipid rafts compared with lipid rafts from wild-type hepatocytes (Table 5). Likewise, SCP-2/SCP-x gene ablation had no effect on these parameters in nonrafts compared with nonrafts from wild-type hepatocytes (Table 5). However, lipid rafts from SCP-2/SCP-x gene-ablated hepatocytes exhibited increased saturated fatty acids and Sat/Unsat ratio concomitant with decreased unsaturated fatty acids, MUFA, and

TABLE 5. Effect of SCP-2/SCP-x gene ablation on phosphatidylethanolamine fatty acid group percentage composition in plasma membrane nonraft and lipid raft fractions

Fatty Acid Group	Nonraft		Raft	
	Wild Type	Knockout	Wild Type	Knockout
Saturated	42 ± 2	45 ± 3	54 ± 2 ^a	61 ± 6 ^b
Unsaturated	58 ± 3	55 ± 3	46 ± 2 ^a	39 ± 3 ^b
MUFA	24 ± 1	25 ± 2	21 ± 1	19 ± 2
PUFA	34 ± 3	29 ± 2	25 ± 1 ^a	20 ± 2
Saturated/unsaturated	0.72 ± 0.04	0.83 ± 0.06	1.18 ± 0.06 ^a	1.6 ± 0.2 ^b
MUFA/saturated	0.57 ± 0.03	0.56 ± 0.04	0.39 ± 0.03 ^a	0.30 ± 0.04 ^b
DBI	1.3 ± 0.1	1.1 ± 0.1	0.9 ± 0.1 ^a	0.8 ± 0.1

Values represent means ± SEM (n = 3–6). See supplementary Table V for the percentage composition of individual phosphatidylethanolamine fatty acids.

^aSignificant difference compared with the plasma membrane nonraft fraction isolated from SCP-2/SCP-x wild-type hepatocytes (*P* < 0.05).

^bSignificant difference compared with the plasma membrane nonraft fraction isolated from SCP-2/SCP-x null hepatocytes (*P* < 0.05).

DBI compared with nonrafts from SCP-2/SCP-x gene-ablated hepatocytes (Table 5). Thus, phospholipids in lipid rafts from wild-type hepatocytes had a higher ratio of saturated to unsaturated fatty acids versus that in nonrafts. SCP-2/SCP-x gene ablation significantly increased the Sat/Unsat ratio in PE, did not change this ratio in SM, PC, or PI, and decreased this ratio in PS from lipid rafts compared with lipid rafts from wild-type hepatocytes.

Fluorescence polarization of DHE in lipid raft and nonraft microdomains

The structural properties of the sterol microenvironment were probed by measuring the fluorescence polarization of DHE (see Materials and Methods). Polarization of DHE, when incorporated into rafts and nonrafts at low amounts to avoid self-quenching as described (12, 13), was significantly higher in lipid rafts compared with nonrafts isolated from wild-type mice (**Table 6**). SCP-2/SCP-x gene ablation had no effect on DHE polarization in lipid raft and nonraft domains (Table 6). Thus, fluorescent sterol sensed a more ordered (higher dehydroergosterol polarization) microenvironment in lipid rafts versus nonrafts, but SCP-2/SCP-x gene ablation had no effect on the order of the sterol environment.

Fluorescence polarization of DPH in lipid raft and nonraft microdomains

DPH is a probe molecule that detects the intermediate liquid-ordered phase present in model membranes (reviewed in Refs. 1, 34) and biological membranes (reviewed in Refs. 1, 13, 31) rich in sphingolipid, cholesterol, and saturated acyl chains (i.e., lipid rafts). DPH fluorescence polarization in lipid rafts, 0.3416 ± 0.0046 (Table 6), was in the same range as that reported previously in lipid rafts from peripheral cells (reviewed in Refs. 1, 13, 31) or model membranes (reviewed in Refs. 1, 34) as being consistent with the presence of an intermediate liquid-ordered phase. In contrast, DPH polarization in nonrafts was significantly lower than in lipid rafts (Table 6), not in the range consistent with the presence of the intermediate liquid-ordered phase. SCP-2/SCP-x gene ablation significantly increased DPH fluorescence polarization in lipid rafts but not in nonrafts (Table 6), suggesting that SCP-2 selectively increased the intermediate liquid-ordered phase in lipid rafts.

Fluorescence polarization of *cis*-parinaric acid and NBD-stearic acid to probe fatty acyl chain structure in lipid rafts and nonrafts

Long (i.e., 18 carbon) straight-chain fatty acids such as the synthetic NBD-stearic acid and the naturally occurring kinked-chain *cis*-parinaric acid probe the acyl chain microenvironment of membrane lipid rafts and nonrafts (1, 13, 31). Fluorescence polarization of NBD-stearic acid and *cis*-parinaric acid were both higher in lipid rafts than in nonrafts (Table 6). SCP-2/SCP-x gene ablation significantly increased the fluorescence polarization of both NBD-stearic acid and *cis*-parinaric acid in lipid rafts but not in nonrafts (Table 6). Thus, the acyl chain microenviron-

TABLE 6. Fluorescence polarization of lipid probes in lipid rafts and nonrafts isolated from primary cultured hepatocytes

Fluorescence Probe	Nonraft		Lipid Raft	
	Wild Type	Knockout	Wild Type	Knockout
Dehydroergosterol	0.3156 ± 0.0064	0.3177 ± 0.0069	0.3522 ± 0.0052 ^a	0.3605 ± 0.0086 ^a
1,6-Diphenyl-1,3,5-hexatriene	0.3335 ± 0.0062	0.3267 ± 0.0037	0.3416 ± 0.0046 ^{a,b}	0.3644 ± 0.0045 ^a
9Z,11E,13E,15Z-Octatetradecanoic acid	0.3247 ± 0.0046	0.3241 ± 0.0032	0.3319 ± 0.0041 ^b	0.3629 ± 0.0028 ^a
12-(N-Methyl)-N-[(7-nitrobenz-2-oxa-1,3-diazol-4-yl)amino]-octadecanoic acid	0.2545 ± 0.0067 ^c	0.2912 ± 0.0036	0.2771 ± 0.0042 ^{a,b}	0.3106 ± 0.0047 ^a
1,6-Diphenyl-1,3,5-hexatrienyl-trimethylammonium	0.2865 ± 0.0032 ^c	0.3284 ± 0.0082	0.3139 ± 0.0043 ^{a,b}	0.3562 ± 0.0052 ^a
1,6-Diphenyl-1,3,5-hexatriene-propionic acid	0.3585 ± 0.0058 ^c	0.3172 ± 0.0073	0.3925 ± 0.0094 ^{a,b}	0.3543 ± 0.0038 ^a

Relative fluorescence polarization values represent means ± SEM (n = 7).

^a P < 0.05 versus nonraft of the same mouse strain.

^b P < 0.05 versus lipid raft of SCP-2/SCP-x null mice.

^c P < 0.05 versus nonraft of SCP-2/SCP-x null mice.

ments sensed by NBD-stearic acid and *cis*-parinaric acid were significantly more rigid (i.e., higher polarization) in lipid rafts than in nonraft microdomains. SCP-2/SCP-x gene ablation significantly rigidified the lipid raft microenvironments, as indicated by increased polarization of these probes.

Fluorescence polarization of leaflet-selective probes (DPH-TMA and DPH-Pro) in lipid rafts and nonrafts

Fluorescence polarization of DPH-TMA was significantly lower than that of the inner leaflet-selective probe DPH-Pro in both lipid rafts and nonrafts (Table 6). Polarization of the outer leaflet-selective probe DPH-TMA was significantly higher in lipid rafts than in nonrafts (Table 6). SCP-2/SCP-x gene ablation increased the polarization of DPH-TMA in lipid rafts as well as nonrafts (Table 6). In contrast, SCP-2/SCP-x gene ablation decreased the polarization of DPH-Pro in lipid rafts as well as nonrafts (Table 6). Thus, these data showed that the inner leaflet of lipid rafts and nonrafts was significantly more ordered (higher polarization) than was the outer leaflet. SCP-2/SCP-x gene ablation increased the polarization of the outer leaflet-selective probe TMA-DPH but decreased that of the inner leaflet-selective probe DPH-Pro in both membrane fractions, such that the ratio of DPH-TMA to DPH-Pro polarization was increased from 0.80 to 1.00 in lipid rafts and from 0.87 to 1.04 in nonrafts. Thus, by increasing the order (DPH-TMA polarization) in the outer leaflet while concomitantly decreasing the order (DPH-Pro) in the inner leaflet, SCP-2/SCP-x gene ablation effectively abolished the normal transbilayer fluidity difference in both rafts and nonrafts.

DISCUSSION

Although liver hepatocytes account for the majority of net cholesterol loss from the body, molecular details of RCT through the hepatocyte plasma membrane are not completely understood. Although plasma membrane microdomains (termed lipid rafts) compartmentalize the

proteins/receptors involved in cholesterol efflux from peripheral cells, little is known about the existence and putative role of lipid rafts in liver hepatocytes. The data presented here contributed significant new findings.

First, lipid rafts exist in hepatocyte plasma membranes, representing 33% of total plasma membrane protein, countering the common misconception that has equated the almost negligible levels of caveolin-1 in liver with a paucity of raft domains. It should be noted that basically similar amounts of lipid rafts are isolated by affinity chromatography from purified plasma membranes of peripheral-type cells such as fibroblasts (12).

Second, key protein components of RCT, including SR-B1, ABCA1, and P-gp, were highly enriched in hepatocyte lipid raft domains, but caveolin-1 was not detected in purified lipid rafts or nonrafts. Thus, lipid rafts from hepatocyte plasma membranes differed significantly from those of peripheral cells. Because caveolin-1 correlates with enhanced cholesterol efflux and the inhibition of HDL-cholesteryl ester uptake from peripheral cells (reviewed in Ref. 1), lack of caveolin-1 in hepatocytes suggests that hepatocytes are thereby optimally positioned to facilitate HDL-cholesterol/cholesteryl ester uptake rather than efflux. For example, model membrane studies show that both spontaneous and SCP-2-mediated cholesterol transfer is slower from more rigid compared with fluid membranes (reviewed in Ref. 53). Because lipid rafts are more rigid than nonrafts, it might be expected that sterol transfer would be faster from nonrafts than from rafts. Based on these and other considerations, it has been postulated that the majority of exported cholesterol is not raft-associated (reviewed in Ref. 54). On the contrary, *in vitro* studies show that both spontaneous and SCP-2-mediated cholesterol transfer are nearly 1 order of magnitude faster from lipid rafts (enriched in RCT proteins such as SR-B1 and caveolin-1) than nonrafts isolated from plasma membranes of cultured liver cell fibroblasts (12). Lipid rafts from cultured primary hepatocytes are also enriched in RCT proteins such as SR-B1, ABCA1, and P-gp, which are known to confer enhanced dynamics to cholesterol because: *i*) SR-B1 (55) and caveolin-1 (56) directly bind

cholesterol; *ii*) ABCA1 (57), SR-B1 (58), P-gp (59), and ABCG1 (54, 60) induce the formation of a mobile cholesterol pool/domain; *iii*) ABCA1 (61) and P-gp (59) both enhance transbilayer cholesterol migration from the cytofacial to the exofacial leaflet; and *iv*) SCP-2 overexpression enhances cholesterol uptake/esterification (62–64), whereas SCP-2/SCP-x gene ablation reduces hepatic cholesterol accumulation (65). Thus, by localizing SR-B1, ABCA1, and P-gp in lipid rafts as well as expressing high levels of SCP-2, liver hepatocytes are optimally positioned to mediate the final steps of RCT.

With regard to compensatory changes in these and other RCT proteins in response to SCP-2/SCP-x gene ablation, plasma membrane transporters (SR-B1, ABCA1, and P-gp) were not upregulated, but at least one intracellular transporter (L-FABP) was upregulated, concomitant with hypersecretion of bile acids and cholesterol (65, 66). Conversely, L-FABP gene ablation decreases biliary cholesterol (67). It should also be noted that potential compensation for SCP-2/SCP-x gene ablation by the upregulation of L-FABP (65) described above may also contribute in part to altered C/P ratios and the modest changes in the fatty acid profiles of phospholipids in lipid rafts. L-FABP is known to stimulate the rate-limiting step in microsomal phospholipid synthesis (i.e., glycerol-3-phosphate acyltransferase) in a highly acyl chain-selective manner (68). The L-FABP-mediated enhancement of phospholipids with select acyl chain profiles may potentially increase the pool of these phospholipids available for lipid raft biogenesis.

Third, SCP-2 was significantly associated with hepatocyte plasma membrane lipid rafts rather than nonrafts. The possibility that SCP-2 potentially replaces/compensates at least in part for the absence of caveolin-1 in hepatocytes by facilitating intracellular cholesterol transfer is supported by both *in vitro* and cultured cell experiments. *i*) SCP-2 differentially enhances cholesterol transfer from isolated plasma membranes and lipid rafts (fibroblasts and MDCK cells) to intracellular membrane fractions *in vitro* (reviewed in Refs. 1, 12, 13). *ii*) SCP-2 overexpression in fibroblasts inhibits cholesterol for efflux to HDL (2). *iii*) SCP-2 is associated with lipid rafts but not nonrafts, suggesting that SCP-2 selectively interacts with an as yet unknown receptor(s) in hepatocyte lipid rafts. SCP-2 is known to interact directly with caveolin-1 at the plasma membrane in caveolin-1-expressing cells (69, 70). However, hepatocyte homogenates, lipid rafts, and nonrafts do not contain caveolin-1 (as shown here). *iv*) Although direct comparison of caveolin-1 and SCP-2 structures (i.e., amino acid sequences) reveals very little similarity (14), these proteins have in common two structurally based functional features that are highly important to their potential roles in RCT. Caveolin-1 binds cholesterol in membranes through an as yet unidentified domain (possibly located in the scaffolding region) and through a chaperone complex, again through an as yet unidentified region. Furthermore, caveolin-1 itself binds/recognizes the scaffolding domain of other caveolin-1 molecules in the plasma membrane, consistent with its putative role in cholesterol trafficking between intracellular sites and

lipid rafts/caveolae at the plasma membrane (reviewed in Ref. 1). Likewise, SCP-2 also binds cholesterol (reviewed in Ref. 1) and interacts directly with caveolin-1, albeit through a totally different site independent of the caveolin-1 scaffolding domain (69, 70).

Fourth, on a mass basis (nmol/mg protein), hepatocyte lipid rafts were found to be highly lipid-rich in total lipid and phospholipids as well as in the following select lipid classes (also typically found in lipid rafts/caveolae of peripheral cells). *i*) Cholesterol and GM1, lipids commonly used as lipid raft markers. Cholesterol and sphingolipids are thought to provide a significant driving force for lipid raft formation (reviewed in Ref. 1). *ii*) Phospholipid classes typically enriched in lipid rafts (especially SM). On a percentage composition basis, the overall relative order of prevalence of phospholipid classes shown here in hepatocyte lipid rafts was PC > SM and PE > PI and PS. *iii*) Esterified saturated fatty acids were enriched in all lipid raft phospholipid classes examined, thereby yielding higher Sat/Unsat ratios for each respective phospholipid class in lipid rafts than for the same class in nonrafts. These results are important because cholesterol exhibits higher affinity for phospholipids with saturated and mono-unsaturated fatty acids versus polyunsaturated fatty acids (reviewed in Ref. 71) and because polyunsaturated fatty acid incorporation into lipid raft phospholipids will dramatically alter lipid raft lipid distribution and protein distribution/function (72). *iv*) The content of polyunsaturated fatty acids was extremely low (near 5%) in SM of lipid rafts. Likewise, the content of polyunsaturated fatty acids was up to 2-fold lower in PS, PC, PI, and PE located in lipid rafts than in the same phospholipid class found in nonrafts isolated from wild-type hepatocytes. These findings are consistent with model membrane studies of phase-separated membranes, in which saturated (or mono-unsaturated) phospholipids partition preferentially into the cholesterol/sphingolipid-rich phase and polyunsaturated phospholipids are excluded (reviewed in Ref. 71). The driving force for this separation is thought to be the poor ability of cholesterol to pack closely with highly “kinked” conformations of polyunsaturated fatty acid chains, compared with the relative ease of cholesterol packing closely with the extended “straight” acyl chains of saturated fatty acids and, to some degree, with monounsaturated fatty acids. *v*) Hepatocyte lipid rafts were rich in lipid classes transported through lipid rafts, including unesterified cholesterol, cholesteryl ester, and unesterified fatty acid. The presence of these lipids in lipid rafts was not, however, attributable to copurification of bound serum lipoproteins or albumin, since Western blotting did not detect apoA-I, apoB, or albumin in lipid rafts or nonrafts (data not shown). Instead, these findings may be rationalized by the fact that cholesterol and cholesteryl ester, both associated with lipoproteins (HDL), are delivered to lipid rafts via HDL binding to SR-B1 (enriched in lipid rafts by 11-fold). The presence of differential amounts of cholesterol and cholesteryl esters in lipid rafts in hepatocyte plasma membranes may be rationalized not only by the lower membrane solubility of cholesteryl esters

than cholesterol but also by the fact that the respective transport pathways for cholesterol and cholesteryl ester differ (reviewed in Ref. 1). Finally, the presence of unesterified fatty acids in lipid rafts correlates with the enrichment of lipid rafts in proteins that bind and transport fatty acids across the plasma membrane (52).


Fifth, hepatocyte lipid raft domains were significantly less fluid than nonrafts. Fluorescence polarizations of essentially all probes examined (DHE, *cis*-parinaric acid, NBD-stearic acid, DPH, DPH-TMA, and DPH-Pro) were all higher in lipid rafts than in nonrafts, indicating that lipid rafts were more ordered (less fluid) than those of nonrafts. Furthermore, the fluorescence polarization of DPH was in the same range as that observed for DPH in the intermediate liquid-ordered phase of model membranes and of lipid rafts from peripheral cells (fibroblasts) (reviewed in Refs. 12, 13, 31). Differences in lipid composition supported the lower fluidity of lipid rafts versus nonrafts from wild-type hepatocytes. *i*) Lipid rafts were enriched in cholesterol and sphingolipids, both of which make membranes less fluid as well as spontaneously form lateral and transbilayer microdomains in model membranes (reviewed in Ref. 1). Furthermore, cholesterol regulates the distribution of proteins either through direct interactions (73) or by making membranes more rigid (less fluid), a structure that largely excludes most proteins (reviewed in Ref. 1). *ii*) SM of lipid rafts was enriched in saturated and monounsaturated fatty acyl chains (together constituting nearly 95% of the total). *iii*) The other phospholipid classes present in lipid rafts were each enriched in saturated and monounsaturated acyl chains, resulting in higher Sat/Unsat ratios, compared with the same phospholipid classes in nonrafts.

Sixth, hepatocyte lipid rafts and nonrafts both exhibited a transbilayer fluidity gradient in which the inner leaflet appeared less fluid (more rigid), as determined by fluorescence polarization of leaflet-selective probe molecules. The molecular basis for the transbilayer fluidity gradient is primarily attributable to the enrichment of cholesterol in the cytofacial (inner) leaflet of the plasma membranes of nucleated cells (reviewed in Refs. 74, 75). The transbilayer fluidity gradient is essential for the optimal function of transbilayer transport processes, as shown for the Na⁺K⁺-ATPase and other receptor-mediated processes (reviewed in Ref. 76).

Seventh, SCP-2/SCP-x gene ablation completely abolished the expression of SCP-2 and significantly altered hepatocyte lipid raft content and protein distribution, consistent with the effects of SCP-2/SCP-x gene ablation on lipid raft lipid composition, fluidity, and transbilayer structure. *i*) SCP-2/SCP-x gene ablation increased the relative proportion of lipid rafts by 1.5-fold compared with nonrafts, reflective of increased levels of SM detected in the lipid raft fraction from SCP-2/SCP-x gene-ablated hepatocytes. Conversely, overexpression of SCP-2 in cultured fibroblasts decreased the proportion of SM in the lipid raft fraction (12). Sphingolipids, rich in saturated and monounsaturated fatty acids, spontaneously form lipid rafts in bilayers containing other phospholipids and

cholesterol (reviewed in Ref. 1), such that treatment with sphingomyelinase disrupts lipid rafts (reviewed in Ref. 54). SCP-2 is known to enhance the transfer of multiple sphingolipid subclasses (SM, glycosphingolipids, gangliosides, etc.), albeit not equally, between membranes *in vitro* (77). Studies of SCP-2-overexpressing liver cell fibroblasts indicate that SCP-2 has the lowest affinity for SM compared with any other sphingolipid subclass examined and preferentially enhances the targeting of other sphingolipid classes to lipid rafts at the expense of SM (78). *ii*) SCP-2/SCP-x gene ablation increased the total amount of ABCA1, SR-B1, and P-gp protein available at the hepatocyte plasma membrane for HDL-mediated cholesterol trafficking by 1.5-fold, but this was attributable primarily to the increased proportion of lipid rafts rather than to the increased rigidity of the lipid rafts in SCP-2/SCP-x gene-ablated hepatocytes. Although the distribution of ABCA1, SR-B1, and P-gp to lipid rafts is known to depend on the presence of cholesterol, neither cholesterol mass nor C/P ratio in lipid rafts was altered by SCP-2/SCP-x gene ablation (shown here with hepatocytes) or SCP-2 overexpression (shown with liver cell fibroblasts) (12). Thus, the amount of lipid raft and, thereby, the amount of liquid-ordered phase in hepatocyte plasma membranes, rather than the degree of rigidity of the lipid raft lipids therein, determined the level of ABCA1, SR-B1, and P-gp per milligram of protein in lipid rafts. In contrast, fluidizing lipid rafts by the incorporation of polyunsaturated fatty acids significantly reduces the distribution of caveolin-1 and other proteins into lipid rafts (72, 79). *iii*) SCP-2/SCP-x gene ablation increased the rigidity (decreased fluidity) in hepatocyte lipid rafts, primarily as a result of the increased content of SM and saturated and monounsaturated acyl chains, consistent with SCP-2's ability to selectively bind/transfer other sphingolipids more effectively than SM (see above). SCP-2 overexpression in liver cell fibroblasts dramatically reduces spontaneous and protein-mediated cholesterol efflux from purified lipid rafts *in vitro* (12) and inhibits HDL-mediated cholesterol efflux from intact living liver cell fibroblasts (2). Although the effect of increased lipid raft rigidity (decreased fluidity) on HDL-mediated cholesterol uptake/efflux in hepatocytes remains to be determined, SCP-2/SCP-x gene ablation reduced hepatic cholesterol and cholesteryl ester content (65), whereas SCP-2 overexpression enhanced hepatic cholesterol accumulation (64). In contrast, incorporation of polyunsaturated fatty acids displaces cholesterol from rafts (80), fluidizes lipid rafts (72, 79), increases ABCA1 degradation (81), and reduces RCT (82). *iv*) SCP-2/SCP-x gene ablation abolished the transbilayer fluidity gradient in lipid rafts of hepatocytes, reflective of the increased exofacial leaflet rigidity (DPH-TMA) concomitant with decreased cytofacial leaflet rigidity (DPH-Pro). In wild-type hepatocytes, the outer (exofacial) leaflet was more fluid than the inner (cytofacial) leaflet, a result also observed in the plasma membrane of peripheral nucleated cell types (41, 83–86) and largely attributable to the enrichment of cholesterol in the cytofacial leaflet (reviewed in Ref. 53). Although the effect of SCP-2 gene ablation on

transbilayer cholesterol distribution is not known, the data regarding phospholipid distribution may help to explain the results observed with the SCP-2/SCP-x gene-ablated hepatocytes. The increased rigidity of the outer leaflet correlated with the increased lipid raft content of SM, a lipid that is known to make membrane more rigid and to be exclusively localized in the exofacial leaflet. In contrast, the three major phospholipids enriched in the cytofacial leaflet are PS, PI, and PE. The decreased rigidity of the cytofacial leaflet of lipid rafts from SCP-2/SCP-x gene-ablated hepatocytes correlated with the higher DBI of PS (those of PI and PE were unchanged). Consistent with the importance of the transbilayer fluidity gradient in receptor-mediated transbilayer transport processes (reviewed in Ref. 76), SCP-2 gene ablation reduces cholesterol absorption and alters biliary cholesterol excretion in liver (87). In contrast, SCP-2 overexpression in cultured fibroblasts alters the structural properties of lipid rafts in plasma membranes (12), enhances HDL-mediated cholesterol uptake for esterification (63), and inhibits cholesterol efflux (2), whereas SCP-2 overexpression in mice enhances hepatic cholesterol accumulation (64). Thus, an important role of SCP-2 within the cell appears to be ensuring the dynamic flow of cholesterol into and out of lipid rafts with cross-talk between SCP-2 and the RCT proteins involved in transmembrane cholesterol transfer and uptake/efflux through a dynamic cholesterol pool within lipid rafts. Consistent with this possibility, studies with liver cell fibroblast lipid rafts and nonrafts show that SCP-2 increases the size of the rapidly transferable sterol domain by 4.2-fold in lipid rafts, but not in nonrafts, in vitro (12).

In summary, the data presented here with SCP-2/SCP-x gene-ablated mice and an affinity chromatography method (detergent-free, high-pH carbonate buffer-free) to simultaneously isolate lipid rafts and nonrafts show for the first time the existence of both lipid rafts and nonrafts in high proportion (1:2) in the plasma membrane of primary hepatocytes. Biochemical and biophysical characterization further revealed that primary hepatocyte lipid rafts exhibited a unique lipid distribution consistent with preferential interaction of cholesterol with select phospholipid classes, a structure consistent with an intermediate liquid-ordered phase, as well as a transbilayer fluidity gradient, enrichment in proteins mediating HDL-cholesterol trafficking, and regulation of these properties by SCP-2 expression. 

This work was supported in part by U.S. Public Health Service, National Institutes of Health Grants GM-31651 and DK-41402 (F.S. and A.B.K.), DK-70965 (B.P.A.), and DK-62812 (A.M.G.). The technical assistance of Mr. Danilo Landrock and Ms. Meredith Dixon is greatly appreciated.

REFERENCES

1. Schroeder, F., B. P. Atshaves, A. M. Gallegos, A. L. McIntosh, J. C. Liu, A. B. Kier, H. Huang, and J. M. Ball. 2005. Lipid rafts and caveolae organization. *In Advances in Molecular and Cell Biology*. P. G. Frank and M. P. Lisanti, editors. Elsevier, Amsterdam, The Netherlands. 3–36.

2. Atshaves, B. P., O. Starodub, A. L. McIntosh, J. B. Roths, A. B. Kier, and F. Schroeder. 2000. Sterol carrier protein-2 alters HDL-mediated cholesterol efflux. *J. Biol. Chem.* **275**: 36852–36861.
3. Matveev, S. V., A. Uittenbogaard, D. R. van der Westhuyzen, and E. J. Smart. 2001. Caveolin-1 negatively regulates SRB1 mediated selective uptake of high density lipoprotein-derived cholesteryl ester. *Eur. J. Biochem.* **268**: 5609–5616.
4. Schmitz, G., W. E. Kaminski, and E. Orso. 2000. ABC transporters in cellular lipid trafficking. *Curr. Opin. Lipidol.* **11**: 493–501.
5. Lavie, Y., and M. Liscovitch. 2000. Changes in lipid and protein constituents of rafts and caveolae in multidrug resistant cancer cells and their functional consequences. *Glycoconj. J.* **17**: 253–259.
6. Malerod, L., L. K. Juvet, T. Gjoen, and T. Berg. 2002. The expression of scavenger receptor class B, type 1 (SRB1) and caveolin in parenchymal and non-parenchymal cells. *Cell Tissue Res.* **307**: 173–180.
7. Vainio, S., S. Heino, J. E. Mansson, P. Fredman, E. Kuismanen, O. Vaarala, and E. Ikonen. 2002. Dynamic association of human insulin receptor with lipid rafts in cells lacking caveolae. *EMBO Rep.* **3**: 95–100.
8. Moreno, M., H. Molina, L. Amigo, S. Zanlungo, S. Arrese, A. Rigotti, and J. F. Miquel. 2003. Hepatic overexpression of caveolin-1 increases bile salt secretion in mice. *Hepatology.* **38**: 1477–1488.
9. Wustner, D., A. Herrmann, M. Hao, and F. R. Maxfield. 2002. Rapid nonvesicular transport of sterol between the plasma membrane domains of polarized hepatic cells. *J. Biol. Chem.* **277**: 30325–30336.
10. Schroeder, F., A. Frolov, J. Schoer, A. Gallegos, B. P. Atshaves, N. J. Stolowich, A. I. Scott, and A. B. Kier. 1998. Intracellular sterol binding proteins, cholesterol transport and membrane domains. *In Intracellular Cholesterol Trafficking*. T. Y. Chang and D. A. Freeman, editors. Kluwer Academic Publishers, Boston, MA. 213–234.
11. Schroeder, F., R. N. Fontaine, and D. A. Kinden. 1982. LM fibroblast plasma membrane subfractionation by affinity chromatography on ConA-Sepharose. *Biochim. Biophys. Acta.* **690**: 231–242.
12. Atshaves, B. P., A. Gallegos, A. L. McIntosh, A. B. Kier, and F. Schroeder. 2003. Sterol carrier protein-2 selectively alters lipid composition and cholesterol dynamics of caveolae/lipid raft vs non-raft domains in L-cell fibroblast plasma membranes. *Biochemistry.* **42**: 14583–14598.
13. Gallegos, A. M., S. M. Storey, A. B. Kier, F. Schroeder, and J. M. Ball. 2006. Structure and cholesterol dynamics of caveolae/raft and nonraft plasma membrane domains. *Biochemistry.* **45**: 12100–12116.
14. Storey, S. M., T. F. Gibbons, C. V. Williams, R. D. Parr, F. Schroeder, and J. M. Ball. 2007. Full-length, glycosylated NSP4 is localized to plasma membrane caveolae by a novel raft isolation technique. *J. Virol.* **81**: 5472–5483.
15. Atshaves, B. P., A. Petrescu, O. Starodub, J. Roths, A. B. Kier, and F. Schroeder. 1999. Expression and intracellular processing of the 58 kDa sterol carrier protein 2/3-oxoacyl-CoA thiolase in transfected mouse L-cell fibroblasts. *J. Lipid Res.* **40**: 610–622.
16. McIntosh, A., B. P. Atshaves, H. Huang, A. M. Gallegos, A. B. Kier, F. Schroeder, H. Xu, W. Zhang, and S. Liu. 2006. Multiphoton laser scanning microscopy and spatial analysis of dehydroergosterol distributions on plasma membranes of living cells. *In Lipid Rafts*. T. McIntosh, editor. Humana Press, Totowa, NJ. 85–105.
17. Atshaves, B. P., A. L. McIntosh, O. I. Lyuksyutova, W. R. Zipfel, W. W. Webb, and F. Schroeder. 2004. Liver fatty acid binding protein gene ablation inhibits branched-chain fatty acid metabolism in cultured primary hepatocytes. *J. Biol. Chem.* **279**: 30954–30965.
18. Lanford, R. E., K. D. Carey, L. E. Estlack, G. C. Smith, and R. V. Hay. 1989. Analysis of plasma protein and lipoprotein synthesis in long term primary cultures of baboon hepatocytes maintained in serum-free medium. *In Vitro Cell. Dev. Biol.* **25**: 174–182.
19. Foster, L. J., C. L. de Hoog, and M. Mann. 2003. Unbiased quantitative proteomics of lipid rafts reveals high specificity for signaling factors. *Proc. Natl. Acad. Sci. USA.* **100**: 5813–5818.
20. Pike, L. J., X. Han, K-N. Chung, and R. W. Gross. 2002. Lipid rafts are enriched in arachidonic acid and plasmenylethanolamine and their composition is independent of caveolin-1 expression: a quantitative electrospray ionization/mass spectrometric analysis. *Biochemistry.* **41**: 2075–2088.
21. Pike, L. J. 2003. Lipid rafts: bringing order to chaos. *J. Lipid Res.* **44**: 655–667.
22. Schagger, H., and G. vonJagow. 1987. Tricine-sodium dodecyl sulfate-polyacrylamide gel electrophoresis for the separation of proteins in the range from 1 to 100 kDa. *Anal. Biochem.* **166**: 368–379.

23. Robertson, D., P. Monaghan, C. Clarke, and A. J. Atherton. 1992. An appraisal of low-temperature embedding by progressive lowering of temperature into Lowicryl HM20 for immunocytochemical studies. *J. Microsc.* **168**: 85–100.
24. Jefferson, J. R., J. P. Slotte, G. Nemezc, A. Pastuszyn, T. J. Scallen, and F. Schroeder. 1991. Intracellular sterol distribution in transfected mouse L-cell fibroblasts expressing rat liver fatty acid binding protein. *J. Biol. Chem.* **266**: 5486–5496.
25. Marzo, A., P. Ghirardi, D. Sardini, and G. Meroni. 1971. Simplified measurement of monoglycerides, diglycerides, triglycerides, and free fatty acids in biological samples. *Clin. Chem.* **17**: 145–147.
26. Hara, A., and N. S. Radin. 1978. Lipid extraction of tissues with a low toxicity solvent. *Anal. Biochem.* **90**: 420–426.
27. Eckert, G. P., U. Igbavboa, W. Muller, and W. G. Wood. 2003. Lipid rafts of purified mouse brain synaptosomes prepared with or without detergent reveal different lipid and protein domains. *Brain Res.* **962**: 144–150.
28. Rouser, G., A. Siakotos, and S. Fleischer. 1969. Quantitative analysis of phospholipids by thin-layer chromatography and phosphorus analysis of spots. *Lipids.* **1**: 85–86.
29. Andrade, C. M. B., V. M. T. Trindade, C. C. A. Cardoso, A. L. Ziulkoski, L. C. Trugo, R. N. Guaragna, R. Borojevic, and F. C. R. Guma. 2003. Changes of sphingolipid species in the phenotype conversion from myofibroblasts to lipocytes in hepatic stellate cells. *J. Cell. Biochem.* **88**: 533–544.
30. Bradford, M. 1976. A rapid and sensitive method for the quantitation of microgram quantities of protein utilizing the principle of protein-dye binding. *Anal. Biochem.* **72**: 248–254.
31. Gallegos, A. M., A. L. McIntosh, B. P. Atshaves, and F. Schroeder. 2004. Structure and cholesterol domain dynamics of an enriched caveolae/raft isolate. *Biochem. J.* **382**: 451–461.
32. McIntosh, A., A. Gallegos, B. P. Atshaves, S. Storey, D. Kannoju, and F. Schroeder. 2003. Fluorescence and multiphoton imaging resolve unique structural forms of sterol in membranes of living cells. *J. Biol. Chem.* **278**: 6384–6403.
33. Schroeder, F., S. C. Myers-Payne, J. T. Billheimer, and W. G. Wood. 1995. Probing the ligand binding sites of fatty acid and sterol carrier proteins: effects of ethanol. *Biochemistry.* **34**: 11919–11927.
34. Brown, D. A., and E. London. 1998. Structure and origin of ordered lipid domains in biological membranes. *J. Membr. Biol.* **164**: 103–114.
35. Schroeder, F. 1988. Use of fluorescence spectroscopy in the assessment of biological membrane properties. In *Advances in Membrane Fluidity: Methods for Studying Membrane Fluidity*. R. C. Aloia, C. C. Cirtain, and L. M. Gordon, editors. Alan R. Liss, New York. 193–217.
36. Wood, W. G., and F. Schroeder. 1992. Membrane exofacial and cytofacial leaflets: a new approach to understanding how ethanol alters brain membranes. In *Alcohol and Neurobiology: Receptors, Membranes, and Channels*. R. R. Watson, editor. CRC Press, Boca Raton, FL. 161–184.
37. Colles, S. M., W. G. Wood, S. C. Myers-Payne, U. Igbavboa, N. A. Avdulov, J. Joseph, and F. Schroeder. 1995. Structure and polarity of mouse brain synaptic plasma membrane: effects of ethanol *in vitro* and *in vivo*. *Biochemistry.* **34**: 5945–5959.
38. Schroeder, F. 1980. Fluorescence probes as monitors of surface membrane fluidity gradients in murine fibroblasts. *Eur. J. Biochem.* **112**: 293–307.
39. Schroeder, F., W. J. Morrison, C. Gorka, and W. G. Wood. 1988. Transbilayer effects of ethanol on fluidity of brain membrane leaflets. *Biochim. Biophys. Acta.* **946**: 85–94.
40. Prendergast, F. G., R. P. Haugland, and P. J. Callahan. 1981. 1-[4-(Trimethylamino)phenyl]-6-phenylhexa-1,3,5-triene: synthesis, fluorescence properties, and use as a fluorescence probe of lipid bilayers. *Biochemistry.* **20**: 7333–7338.
41. Wisniewski, B. J., and K. K. Iwata. 1977. Electron spin resonance evidence for vertical asymmetry in animal cell membranes. *Biochemistry.* **16**: 1321–1326.
42. van Dijk, P. W. M., E. J. J. van Zoelen, R. Seldenrijk, L. L. M. van Deenen, and J. D. Gier. 1976. Calorimetric behaviour of individual phospholipid classes from human and bovine erythrocyte membranes. *Chem. Phys. Lipids.* **17**: 336–343.
43. Daleke, D. L. 2003. Regulation of transbilayer plasma membrane phospholipid asymmetry. *J. Lipid Res.* **44**: 233–242.
44. Daleke, D. L. 2007. Phospholipid flippases. *J. Biol. Chem.* **282**: 821–825.
45. Harder, T., P. Schieffele, P. Verkade, and K. Simons. 1998. Lipid domain structure of the plasma membrane revealed by patching of membrane components. *J. Cell Biol.* **141**: 929–942.
46. Nichols, B. 2003. Caveosomes and endocytosis of lipid rafts. *J. Cell Sci.* **116**: 4707–4714.
47. Allen, J. A., J. Z. Yu, R. J. Donati, and M. M. Rasenick. 2005. Beta-Adrenergic receptor stimulation promotes G alpha internalization through lipid rafts: a study in living cells. *Mol. Pharmacol.* **67**: 1493–1504.
48. Ehehalt, R., P. Keller, C. Haass, C. Thiele, and K. Simons. 2003. Amyloidogenic processing of the Alzheimer beta-amyloid precursor protein depends on lipid rafts. *J. Cell Biol.* **160**: 113–123.
49. Damjanovich, S., L. Matyus, L. Damjanovich, L. Bene, A. Jenei, J. Matko, R. Gaspar, and J. Szollosi. 2007. Does mosaicism of the plasma membrane at molecular and higher hierarchical levels in human lymphocytes carry information on the immediate history of cells? *Immunol. Lett.* **82**: 93–99.
50. Calvo, M., and C. Enrich. 2000. Biochemical analysis of a caveolae-enriched plasma membrane fraction from rat liver. *Electrophoresis.* **21**: 3386–3395.
51. Shaul, P. W., and K. L. Chambliss. 2005. Caveolae and estrogen receptor signaling. In *Caveolae and Lipid Rafts: Roles in Signal Transduction and the Pathogenesis of Human Disease*. M. P. Lisanti and P. G. Frank, editors. Elsevier Academic Press, San Diego, CA. 109–123.
52. Ehehalt, R., J. Fullekrug, J. Pohl, A. Ring, T. Herrmann, and W. Stremmel. 2006. Translocation of long chain fatty acids across the plasma membrane—lipid rafts and fatty acid transport proteins. *Mol. Cell. Biochem.* **284**: 135–140.
53. Schroeder, F., J. R. Jefferson, A. B. Kier, J. Knittell, T. J. Scallen, W. G. Wood, and I. Hapala. 1991. Membrane cholesterol dynamics: cholesterol domains and kinetic pools. *Proc. Soc. Exp. Biol. Med.* **196**: 235–252.
54. Jessup, W., I. Gelissen, K. Gaus, and L. Kritharides. 2006. Roles of ATP binding cassette transporters A1 and G1, scavenger receptor BI and membrane lipid domains in cholesterol export from macrophages. *Curr. Opin. Lipidol.* **17**: 247–267.
55. Assanases, C., C. Mineo, D. Seetharam, I. S. Yuhanna, Y. L. Marcel, M. A. Connelly, D. L. Williams, M. de la Llera-Moya, P. W. Shaul, and D. L. Silver. 2005. Cholesterol binding, efflux, and PDZ-interacting domain of scavenger receptor-B1 mediate HDL-initiated signaling. *J. Clin. Invest.* **115**: 969–977.
56. Fielding, P. E., P. Chau, D. Liu, T. A. Spencer, and C. J. Fielding. 2004. Mechanism of platelet derived growth factor dependent caveolin-1 phosphorylation: relationship to sterol binding and the role of serine-80. *Biochemistry.* **43**: 2578–2586.
57. Oram, J. F. 2003. HDL apolipoproteins and ABCA1. *Arterioscler. Thromb. Vasc. Biol.* **23**: 720–727.
58. Parathath, S., M. A. Connelly, R. A. Rieger, S. M. Klein, N. A. Abumrad, M. de la Llera-Moya, C. R. Iden, G. H. Rothblat, and D. L. Williams. 2004. Changes in plasma membrane properties and phosphatidylcholine subspecies of insect Sf9 cells due to expression of scavenger receptor class B, type 1, and CD36. *J. Biol. Chem.* **279**: 41310–41318.
59. Garrigues, A., A. E. Escargueil, and S. Orlowski. 2002. The multi-drug transporter, P-glycoprotein, actively mediates cholesterol redistribution in the cell membrane. *Proc. Natl. Acad. Sci. USA.* **99**: 10347–10352.
60. Oram, J. F., and A. M. Vaughan. 2006. ATP-binding cassette cholesterol transporters and cardiovascular disease. *Circ. Res.* **99**: 1031–1043.
61. Ikeda, M., A. Kihara, and Y. Igarashi. 2006. Lipid asymmetry of the eukaryotic plasma membrane: functions and related enzymes. *Biol. Pharm. Bull.* **29**: 1542–1546.
62. Moncecchi, D. M., E. J. Murphy, D. R. Prows, and F. Schroeder. 1996. Sterol carrier protein-2 expression in mouse L-cell fibroblasts alters cholesterol uptake. *Biochim. Biophys. Acta.* **1302**: 110–116.
63. Murphy, E. J., and F. Schroeder. 1997. Sterol carrier protein-2 mediated cholesterol esterification in transfected L-cell fibroblasts. *Biochim. Biophys. Acta.* **1345**: 283–292.
64. Amigo, L., S. Zanlungo, J. F. Miquel, J. M. Glick, H. Hyogo, D. E. Cohen, A. Rigotti, and F. Nervi. 2003. Hepatic overexpression of sterol carrier protein-2 inhibits VLDL production and reciprocally enhances biliary lipid secretion. *J. Lipid Res.* **44**: 399–407.
65. Seedorf, U., M. Raabe, P. Ellinghaus, F. Kannenberg, M. Fobker, T. Engel, S. Denis, F. Wouters, K. W. A. Wirtz, R. J. A. Wanders, et al. 1998. Defective peroxisomal catabolism of branched fatty acyl coenzyme A in mice lacking the sterol carrier protein-2/sterol carrier protein-x gene function. *Genes Dev.* **12**: 1189–1201.

66. Puglielli, L., A. Rigotti, L. Amigo, L. Nunez, A. V. Greco, M. J. Santos, and F. Nervi. 1996. Modulation on intrahepatic cholesterol trafficking: evidence by *in vivo* antisense treatment for the involvement of sterol carrier protein-2 in newly synthesized cholesterol transfer into bile. *Biochem. J.* **317**: 681–687.
67. Martin, G. G., H. Danneberg, L. S. Kumar, B. P. Atshaves, E. Erol, M. Bader, F. Schroeder, and B. Binas. 2003. Decreased liver fatty acid binding capacity and altered liver lipid distribution in mice lacking the liver fatty acid binding protein (L-FABP) gene. *J. Biol. Chem.* **278**: 21429–21438.
68. Jolly, C. A., E. J. Murphy, and F. Schroeder. 1998. Differential influence of rat liver fatty acid binding protein isoforms on phospholipid fatty acid composition: phosphatidic acid biosynthesis and phospholipid fatty acid remodeling. *Biochim. Biophys. Acta.* **1390**: 258–268.
69. Zhou, M., R. D. Parr, A. D. Petrescu, H. R. Payne, B. P. Atshaves, A. B. Kier, J. A. Ball, and F. Schroeder. 2004. Sterol carrier protein-2 directly interacts with caveolin-1 *in vitro* and *in vivo*. *Biochemistry.* **43**: 7288–7306.
70. Parr, R. D., G. G. Martin, H. A., Hostetler, M. E., Schroeder, K. D., Mir, A. B., Kier, J. M., Ball, and F. Schroeder. 2007. A new N-terminal recognition domain in caveolin-1 interacts with sterol carrier protein-2 (SCP-2). *Biochemistry.* **46**: 8301–8314.
71. Shaikh, S. R., A. C. Dumauval, A. Castillo, D. LoCascio, R. A. Siddiqui, W. Stillwell, and S. R. Wassall. 2004. Oleic and docosahexaenoic acid differentially phase separate from lipid raft molecules: a comparative NMR, DSC, AFM, and detergent extraction study. *Biophys. J.* **87**: 1752–1766.
72. Siddiqui, R. A., K. A. Harvey, G. P. Zaloga, and W. Stillwell. 2007. Modulation of lipid rafts by ω -3 fatty acids in inflammation and cancer: implications for use of lipids during nutrition support. *Nutr. Clin. Pract.* **22**: 74–88.
73. Burger, K., G. Gimpl, and F. Fahrenholz. 2000. Regulation of receptor function by cholesterol. *Cell. Mol. Life Sci.* **57**: 1577–1592.
74. Schroeder, F. 1981. Use of a fluorescent sterol to probe the transbilayer distribution of sterols in biological membranes. *FEBS Lett.* **135**: 127–130.
75. Hale, J. E., and F. Schroeder. 1982. Asymmetric transbilayer distribution of sterol across plasma membranes determined by fluorescence quenching of dehydroergosterol. *Eur. J. Biochem.* **122**: 649–661.
76. Schroeder, F., and W. D. Sweet. 1988. The role of membrane lipid and structure asymmetry on transport systems. In *Advances in Biotechnology of Membrane Ion Transport*. P. L. Jorgensen and R. Verna, editors. Serono Symposia, New York. 183–195.
77. Bloj, B., and D. B. Zilversmit. 1981. Accelerated transfer of neutral glycosphingolipids and ganglioside GM1 by a purified lipid transfer protein. *J. Biol. Chem.* **256**: 5988–5991.
78. Atshaves, B. P., J. R. Jefferson, A. L. McIntosh, B. M. McCann, K. Landrock, A. B. Kier, and F. Schroeder. 2007. Effect of sterol carrier protein-2 expression on sphingolipid distribution in L-cell fibroblast plasma membrane lipid rafts/caveolae. *Lipids*. In press.
79. Ma, D. W. L., J. Seo, L. A. Davidson, E. S. Callaway, Y.-Y. Fan, J. R. Lupton, and R. S. Chapkin. 2004. n-3 PUFA alter caveolae lipid composition and resident protein localization in mouse colon. *FASEB J.* **18**: 1040–1042.
80. Park, E. J., M. Suh, B. Thomson, A. B. R. Thomson, K. S. Ramanujam, and M. T. Clandinin. 2005. Dietary ganglioside decreases cholesterol content, caveolin expression and inflammatory mediators in rat intestinal microdomains. *Glycobiology.* **15**: 935–942.
81. Brousseau, M. E. 2003. ATP-binding cassette transporter A1, fatty acids, and cholesterol absorption. *Curr. Opin. Lipidol.* **14**: 35–40.
82. Uehara, Y., S. Muira, A. von Eckardstein, S. Abe, A. Fujii, Y. Matsuo, S. Rust, S. Lorkowski, G. Assmann, T. Yamada, et al. 2007. Unsaturated fatty acids suppress the expression of the ATP-binding cassette transporter G1 (ABCG1) and ABCA1 genes via an LXR/RXR responsive element. *Atherosclerosis.* **191**: 11–21.
83. Kirsch, C., G. P. Eckert, and W. E. Mueller. 2002. Statins affect cholesterol micro-domains in brain plasma membranes. *Biochem. Pharmacol.* **65**: 843–856.
84. Igbavboa, U., N. A. Avdulov, F. Schroeder, and W. G. Wood. 1996. Increasing age alters transbilayer fluidity and cholesterol asymmetry in synaptic plasma membranes of mice. *J. Neurochem.* **66**: 1717–1725.
85. Dudeja, P. K., J. M. Harig, R. K. Wali, S. M. Knaup, K. Ramaswamy, and T. A. Brasitus. 1991. Differential modulation of human small intestinal brush-border membrane hemileaflet fluidity affects leucine aminopeptidase activity and transport of D-glucose and L-glutamate. *Arch. Biochem. Biophys.* **284**: 338–345.
86. Morse, P. D., M. Ruhlig, W. Snipes, and A. D. Keith. 1975. *Arch. Biochem. Biophys.* **168**: 40–50.
87. Seedorf, U., M. Raabe, M. Fobker, F. Kannenberg, P. Brysch, J. Engel, N. Maeda, and G. Assmann. 1995. Reduced absorption and hepatic esterification of dietary cholesterol in mice lacking sterol carrier protein-2 and sterol carrier protein-x. *Circulation.* **92**: 2037, Suppl. S.